NPS69-88-001

NAVAL POSTGRADUATE SCHOOL

Monterey, California

TVC JET VANE THERMAL MODELING USING PARAMETRIC SYSTEM IDENTIFICATION

by

ROBERT H. NUNN

Prepared for: Naval Weapons Center
China Lake, CA 93555

NAVAL POSTGRADUATE SCHOOL
Monterey, California

Rear Admiral R. C. Austin
Superintendent

K. T. Marshall
Acting Provost

The work reported here was supported by the Naval Weapons Center, China Lake.

This report was prepared by:

Robert H. Nunn
Professor of Mechanical Engineering

Reviewed by:

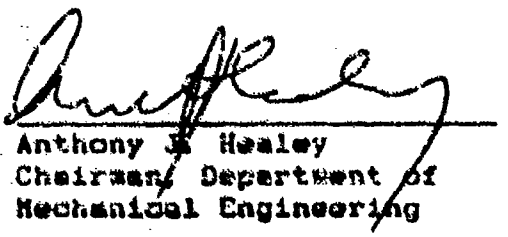

Anthony J. Healey
Chairman, Department of
Mechanical Engineering

Released by:

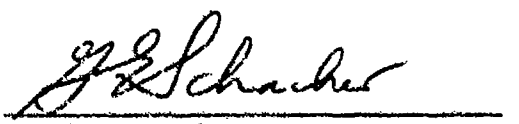

Gordon E. Schacher
Dean of Science and Engineering

UNCLASSIFIED

SECURITY CLASSIFICATION OF THIS PAGE

A191 51

REPORT DOCUMENTATION PAGE

1a REPORT SECURITY CLASSIFICATION UNCLASSIFIED	1b RESTRICTIVE MARKINGS
2a SECURITY CLASSIFICATION AUTHORITY	3 DISTRIBUTION/AVAILABILITY OF REPORT Approved for public release; distribution is unlimited.
2b DECLASSIFICATION/DOWNGRADING SCHEDULE	
4 PERFORMING ORGANIZATION REPORT NUMBER(S) NPS69-88-001	5 MONITORING ORGANIZATION REPORT NUMBER(S)
6a NAME OF PERFORMING ORGANIZATION Naval Postgraduate School	6b OFFICE SYMBOL (If applicable)
6c ADDRESS (City, State, and ZIP Code) Monterey, CA 93943-5100	7b ADDRESS (City, State, and ZIP Code) China Lake, CA 93955
8a NAME OF FUNDING/SPONSORING ORGANIZATION Naval Weapons Center	8b OFFICE SYMBOL (If applicable)
8c ADDRESS (City, State, and ZIP Code) China Lake, CA 93555	9 PROCUREMENT INSTRUMENT IDENTIFICATION NUMBER O&MN, Direct Funding
	10 SOURCE OF FUNDING NUMBERS PROGRAM ELEMENT NO / PROJECT NO / TASK NO / WORK UNIT ACCESSION NO

11 (Include Security Classification)
TVC Jet Vane Thermal Modeling Using Parametric System Identification

12 PERSONAL AUTHOR(S)
Robert H. Nunn

13a TYPE OF REPORT	13b TIME COVERED FROM ... TO	14 DATE OF REPORT (Year, Month, Day)	15 PAGE COUNT
		18 March, 1988	60

16 SUPPLEMENTARY NOTATION

17 COSATI CODES FIELD	GROUP	SUB-GROUP

18 SUBJECT TERMS (Continue on reverse if necessary and identify by block number)

19 ABSTRACT (Continue on reverse if necessary and identify by block number)

Parametric system identification procedures, using the software package MATRIXx, are applied to the problem of simulating the thermal response of a TVC jet vane. The jet vane is discretized into thermal lumps and energy balances are written to develop the governing mathematical relationships. Boundary layer convection and stagnation point heating are considered as thermal inputs, and the associated resistances are estimated. System identification is used to determine the appropriate values for the convective resistances and the vane mount thermal sink. The identified model, which is linear time-variant, closely predicts the thermal response of the jet vane shaft, surface, and tip.

thrust vector control system

20 DISTRIBUTION/AVAILABILITY OF ABSTRACT	21 ABSTRACT SECURITY CLASSIFICATION
☒ UNCLASSIFIED/UNLIMITED ☐ SAME AS RPT ☐ DTIC USERS	UNCLASSIFIED
22a NAME OF RESPONSIBLE INDIVIDUAL	22b TELEPHONE (Include Area Code) / 22c OFFICE SYMBOL

DD FORM 1473, 84 MAR — 83 APR edition may be used until exhausted. All other editions are obsolete.

SECURITY CLASSIFICATION OF THIS PAGE

UNCLASSIFIED

Naval Postgraduate School
Monterey, California

TVC JET VANE THERMAL MODELING USING PARAMETRIC SYSTEM IDENTIFICATION

I. INTRODUCTION

Jet Vane TVC Systems

Thrust vector control (TVC) systems offer means of flight vehicle trajectory control that are virtually independent of external forces. Such a capability is frequently required for tactical missiles, as well as spacecraft launch vehicles, when the relative flow past external lifting surfaces is insufficient to generate the necessary control forces. This commonly occurs during low-speed operations, such as at launch or during hovering flight. High angle of attack flight may also lead to situations in which conventional lifting surfaces are inadequate. In addition, there are occasions when external steering devices are infeasible from a design point of view, such as for tube-launched devices.

Several methods of TVC have been developed and applied to operational and experimental vehicles. These include movable nozzles, internal fluid injection (secondary injection), and mechanical jet deflection systems. Jet vane systems fall in the latter category and they tend to be favored for volume-limited applications requiring relatively low actuation torques, large thrust deflection angles, and rapid response. Jet vanes may also be used with relative

ease to generate roll torques. The application of jet vane TVC dates back to the rockets designed by Goddard, and has extended to the Redstone, Sergeant, Talos, Pershing, and Algo II and III motors [1,2], as well as several installations in smaller tactical rockets.

Of course, there are disadvantages accompanying the selection of jet vanes for TVC purposes. These include thrust losses on the order of 3-5% with undeflected vanes [2]. In addition, the attainment of relatively high thrust deflection angles may lead to axial thrust losses of the same order of magnitude as the resulting side force. However, the chief problem associated with the use of jet vanes is the large thermal loading that they experience as they are required to operate in hot, high-speed, particle-laden flows. This problem leads to design limitations so that jet vanes are often restricted to short-duration use in motors with low-temperature non-metalized propellants.

The aerodynamic (side-force producing) characteristics of jet vanes may be calculated with fair certainty on the basis of inviscid flow theory with suitable corrections for viscous effects [2,3]. On the other hand, difficulties that stem from the severity of the jet-vane thermal environment have led to design practices that are based largely upon past experience and cut-and-try methods. Over-design is therefore inevitable, with virtually no capacity for design optimization. In order to exploit the several advantages of jet vane TVC systems, therefore, it has become necessary to

build reliable data bases and, to the extent possible, attain a fundamental understanding of the heat transfer characteristics of such systems.

This need has led to the work undertaken at the Naval Postgraduate School (NPS) in support of a larger program at the Naval Weapons Center (NWC). Previous investigations at NPS have included applications of computational fluid dynamics (CFD) [4,5] and wind-tunnel tests using infra-red thermography [6]. A summary of the results of these studies, together with an overview of relevant previous works, are contained in Ref. [7]. Work in the area of CFD has continued [8] and recent results [9] have shown that dynamic simulation methods hold promise in further identifying the dominant factors affecting the thermal characteristics of jet vanes. This latter area of study has advanced to the application of parametric system identification, and it is the results of these efforts that are the main subject of this report.

The Jet Vane Thermofluid Environment

In the design of a jet vane system, the integrity of the vanes themselves must be guaranteed over the specified work cycle. Although this is a serious challenge, designers must also consider the behavior of the vanes and supporting structure during transient events. Upon motor ignition, localized jet vane temperatures may rise to near-stagnation values within a few seconds. Temperatures in the vane attachment device will rapidly follow this rise, and severe

thermal stresses may develop due to the proximity of a relatively cool supporting structure. These and other design aspects can only be addressed with precision if there is a good understanding of the convective heat transfer process that gives rise to the energy transfer from the flowing gases to the the vane. Put another way, the application of complex computer codes for thermal conduction in the vane and supporting structure can only follow the specification of the convective boundary conditions.

With respect to these conditions, the problem is even more complex. The vane is immersed in a flow field that is, if generally described, compressible, turbulent, multi-component (and possibly multi-phase), three-dimensional, and unsteady, with variable properties and nonlinear and time-variant boundary conditions. Even if taken one at a time, these complexities present problems that are beyond the state-of-the-art for exact solution. In addition, the overall flow field will contain intersecting and impinging shock waves that give rise to discontinuous events and further complication of the boundary conditions. The presence of various protuber-ances only serves to exacerbate these difficulties.

To further define the problem, it may be of use to consider the levels of heat transfer that might be expected from the point of view of "simple" convection from a supersonic flow to a cooled wall. The convective heat transfer coefficient (h) may be described in terms of the nondimen-

sional Stanton number (St) as follows:

$$h = (\rho V c_p)\, St$$

where ρ, V, and c_p are the density, velocity, and specific heat at constant pressure of the flowing gas. On the assumption that the gas behaves ideally, this expression may be written

$$h = St \left(\frac{k}{k-1} \frac{P}{T} g\, I_{sp}\right)$$

where P and T are local gas pressure and temperature and I_{sp} is the specific impulse. Consider, for instance, the conditions at the exit of a rocket nozzle flowing at Mach 3. With a ratio of specific heats assumed to be k = 1.2, we have, approximately:

$$h = St \left(0.25 \frac{P_o}{T_o} g\, I_{sp}\right)$$

where the subscript ($_o$) refers to stagnation conditions. If a typical case is taken to be given by P_o = 100 bar, T_o = 2560 K, and I_{sp} = 250 s, then, in round numbers, the heat transfer coefficient, in units of (kW/m²K), is h = 2000 St.

In rocket engine nozzles, a typical value for the Stanton number is about 0.002 [10]. Thus, with the result above, the expected value of the heat transfer coefficient is on the order of 4 kW/m²K. Such a value should not be taken as conservative, since actual motor conditions may be more severe and local regions (e.g. stagnation points or regions of flow reversal) may experience much higher values. By way of comparison, values of h such as these are much

larger than those usually considered for convective heat transfer and, in fact, they are more typical of those realized in phase-change processes [11].

II. MODELING AND SIMULATION

Background

A general goal of jet vane heat transfer studies is to develop a capability by which the transient thermal behavior of the vane may be predicted with confidence. An understanding of the energy transport processes occurring at the boundaries of the vane is, of course, essential to the achievement of this goal but, because of the complexity of the thermofluid environment in which the vane operates, CFD methods cannot be expected to yield a complete and comprehensive predictive capability. In addition, the results of CFD modeling must invevitably be simplified if they are to be adapted to vane design purposes and the prediction of system performance. In order to complement the CFD studies, therefore, a program has been initiated to approach the problem from a less-general but more-practical point of view. Underlying this approach is an acceptance of the fact that details of the energy transport processes will never be fully defined. On the other hand, there is also the recognition that the cumulative or "lumped" effect of all the various complications mentioned above is to transfer energy to and from the vane. These boundary processes lead to further energy flow within the vane that ultimately gives

rise to a vane temperature distribution that varies with time.

This transient behavior should reflect the nature of the boundary heat transfer processes that drive it, as well as the thermal impact of various vane design parameters (thermal conductivity, heat capacity, density, geometry, etc.). The transient response is the "signature" of the combined effects of the thermal environment and the vane configuration. This premise is the basis for justification of the modeling and simulation (M&S) study described in subsequent sections of this report.

The goal of the M&S study has been to develop a dynamic model of vane heating and cooling. If such a model can be constructed, even though it is approximate, then significant benefits will accrue. For instance, measured vane temperature histories can be used for deductive purposes such as parametric system identification (PSI) whereby the model is used to deduce what would have had to be true in order for the observed temperature history to have occurred. Having estimated the values of appropriate parameters, local temperatures can be deduced at points in the vane structure where conditions (accessibility, sensor survival, etc.) preclude measurement. In addition, a trustworthy predictive model would: (1) reduce the occasions in which testing is required to verify the effects of design changes, (2) permit the extension of sub-scale test data to predict full scale jet vane performance, and (3) indicate the design directions

most likely to lead to optimum system performance.

Approach

The M&S approach may be thought of as a vast simplification of a numerical model that, were it possible to construct, would lead to a successful predictive capability. Whereas such a comprehensive model would treat the flow environment of the vane and the vane itself in fine numerical detail, the M&S method assumes that sufficient accuracy may be obtained if the flow and the vane are made up of a relatively few thermal parts. An important product of the M&S approach is the prediction of the time history of the vane temperature -- in fact, this is what provides the vital clues that are used to estimate the values of the model parameters.

The system identification procedures used in this study are those familiar to the discipline of automatic controls. If the governing mathematical relationships can be cast in a transfer-function or other systematic form (not necessarily linear), then experimental observations can be related to the various parameters of the model by system identification methods. In order for this procedure to be of value, however, the afore-mentioned parameters must be related to the physical quantities affecting the thermal transport process. The establishment of these relationships is described in the next section of this report.

III. MODEL DISCRETIZATION

The model as presently configured considers only two thermal energy input processes: forced convection at the vane surface and stagnation-point heat transfer at the leading edge. These processes are driven by the flow stagnation temperature which is, in turn, derived from the measured thrust levels by means of the rocket-motor ballistic characteristics. The rise and fall of the stagnation temperature is assumed to follow that of the thrust without significant dynamic offset. In other words, the generic product of the model is a series of functions that give local vane temperatures in response to thrust. (If these functions were linear, they would have direct transfer-function counterparts.)

Several vane discretization schemes have been tested, and it has been found that four "lumps" are sufficient to indicate the general thermal behavior of the vane: vane tip, vane body, shaft, and mount. This configuration leads to a simplicity that is a necessary feature of the M&S approach, and results to be described later justify the use of such simple models as design tools.

Estimation of Geometrical and Thermal Properties

As a preliminary step in the study, the actual vane design of interest to the Naval Weapons Center was configured as a collection of lumps with geometries suitable for estimation of thermal conduction properties. Figure 1 illustrates the vane geometry that has been modeled (the vane

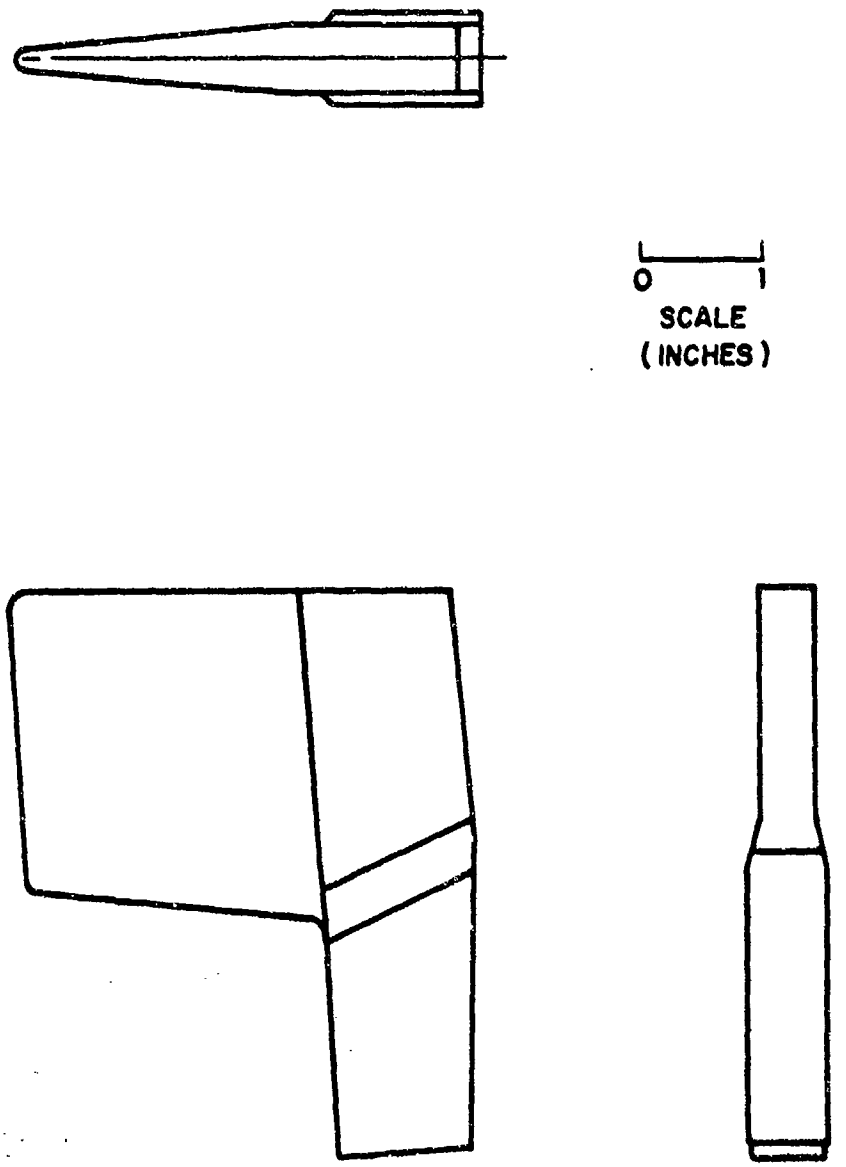

Figure 1. Naval Weapons Center jet vane configuration.

is constructed of 10%Cu/W, and the mount material is steel).

From this design, the fictitious thermal vane has been hypothesized as consisting of three rectangular solids: tip, fin, and shaft. This discretized vane is shown in Fig. 2. The tip of the vane has been separately identified in order to account for the stagnation properties of the thermal convection near the vane leading edge. This portion has been arbitrarily sized so as to have a chord length of 10% of the total vane chord of 3.75 inches. With this length fixed, the discretized tip is shaped so as to have the same lateral area (chord x thickness) as that of the actual tapered and rounded tip.

The remainder of the discretized fin is assumed to be subjected to thermal convection of a turbulent boundary layer type. It is lumped into a rectangular solid of thickness equal to the average value of the tapered fin (with tip removed) and span equal to the mean span of the actual fin. The remaining length dimension is set by equating the volume of the rectangular solid to that of the fin (less the tip portion). The vane shaft is similarly "molded" into a rectangular solid, and this element is assumed to be subjected only to conduction (and radiation, were it included) heat transfer.

The vane mount (not shown in Figs. 1 & 2) is a relatively massive and complex structure. In order to pursue the basic feasibility of the method, no attempt was made to model the thermal resistance of this component in detail.

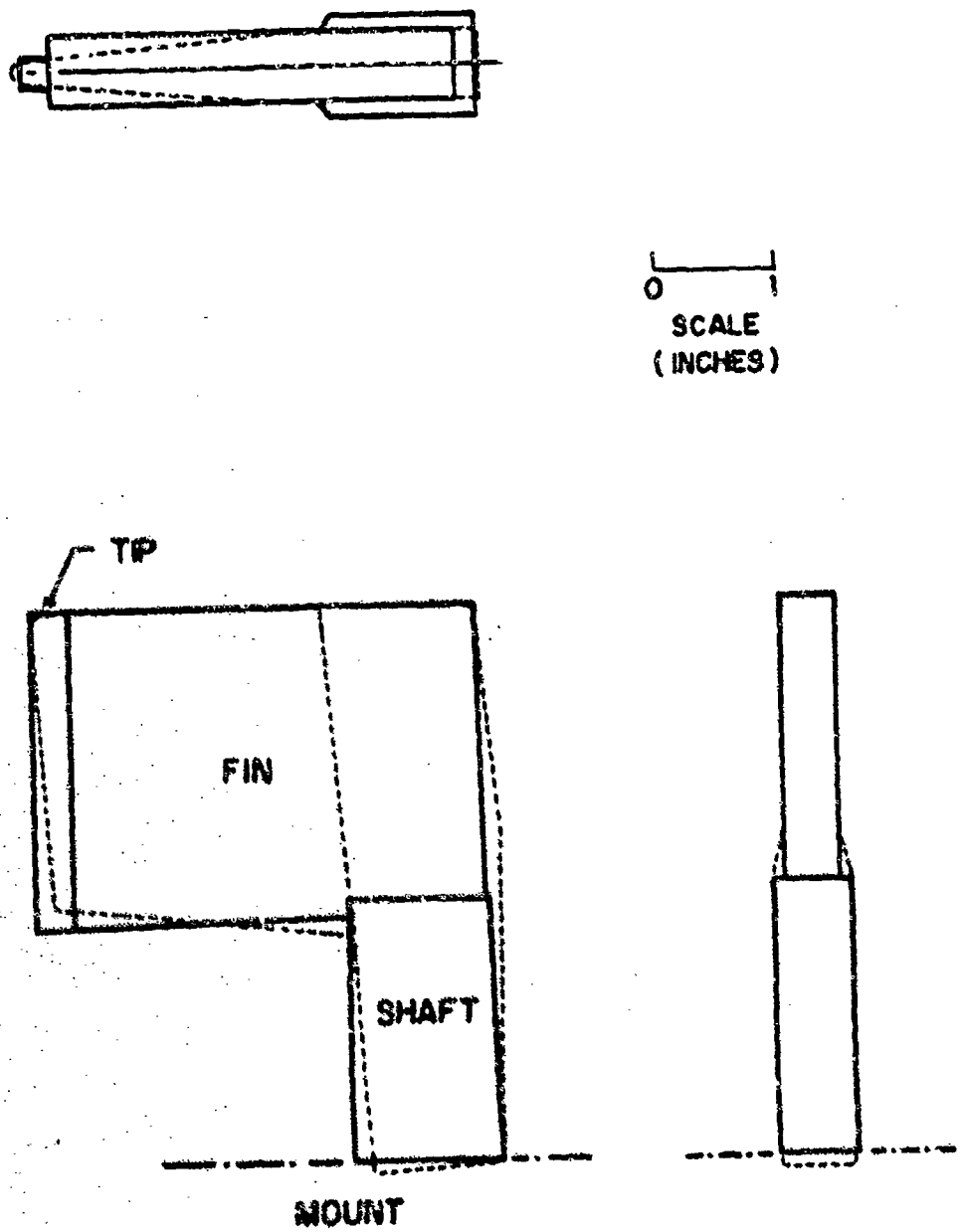

Figure 2. Discretized version of NWC jet vane.

instead, representative sets of values (conduction length and cross-section) for the main mount components were estimated using a rough scaling procedure. The appropriate thermal resistance of the mount was then computed from an analysis of the analogous electrical circuit. In preliminary studies the mount thermal resistance was considered to be an "adjustable parameter" for use in seeking agreement with the available experimental evidence. (Determination of the correct value of this quantity is one of the goals of the system identification procedure described later.)

Each of the components described above was assigned a thermal node located at it's mass-center which, in turn, is the assumed location of the energy storage associated with the entire mass. The capacity to store energy was calculated in the usual way for each lump. For the mount, the thermal capacity was assumed to be infinite -- thus the temperature of this node remained constant at ambient (ground) temperature during the simulation.

It should be emphasized that at this point in the study the discretization rationale is quite arbitrary -- the goal has been to obtain adequate agreement with test results using the minimum number of thermal components. Refinement of the model can easily include the division of the vane structure into a larger number of smaller "lumps." Although this would permit the estimation of temperatures at more nodes and interfaces, the accuracy of these estimates would be no greater than that associated with the "minimum node"

model described here. Such added complication of the vane nodal distribution would only be justifiable in conjunction with a more-detailed description of the thermal boundary conditions, and this would add even more uncertainty to the model. Results described later indicate that such complication is not necessary.

Development of the Governing Equations

With the thermal network and associated properties thus defined, the governing equations were formulated by means of an energy balance at each node. In general, this balance reads "rate of heat flow in = rate of heat flow out + rate of energy storage." For the fin node (node 2 in Fig.3), for instance:

$$\frac{T_{R2} - T_2}{R_{F2}} + \frac{T_1 - T_2}{R_{12}} = \frac{T_2 - T_3}{R_{23}} + C_2 s T_2 \qquad (1)$$

Here the symbol R is used to denote thermal resistance -- 1/hA for convection to the fin and L/kA for conduction between the nodes -- and C is thermal capacitance (mass x heat capacity). The letter s is, as usual, the symbol for the Laplace variable. Calculation of the recovery temperature T_{R2} is discussed in the next section.

The temperature at the node may be expressed explicitly in terms of the surrounding nodal temperatures as follows:

$$T_2 = \frac{R_{n2}}{1 + \tau_2 s}\left(\frac{T_{R2}}{R_{F2}} + \frac{T_1}{R_{12}} + \frac{T_3}{R_{23}}\right) \qquad (2)$$

where the nodal resistance R_{n2} is given by:

$$\frac{1}{R_{n2}} = \frac{1}{R_{F2}} + \frac{1}{R_{12}} + \frac{1}{R_{23}}$$

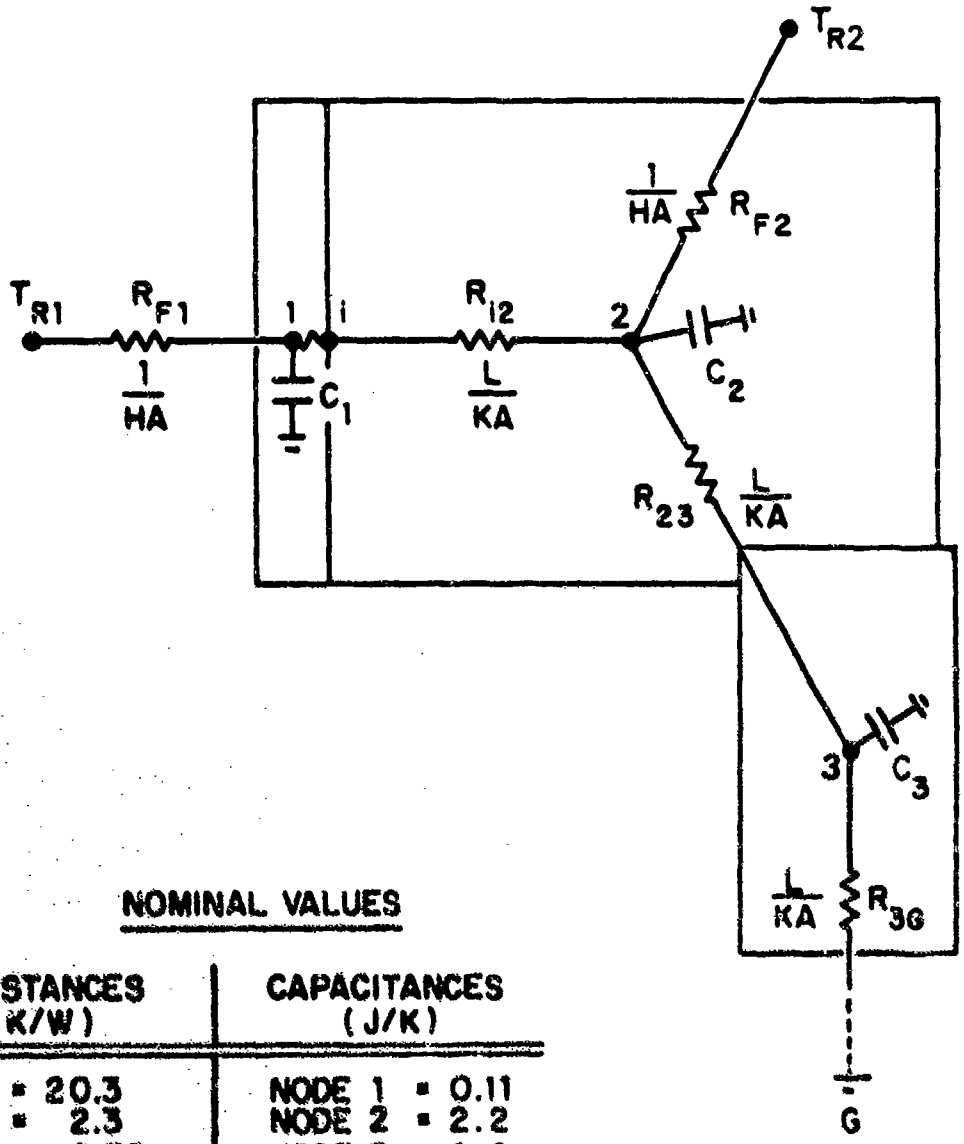

NOMINAL VALUES

RESISTANCES (K/W)	CAPACITANCES (J/K)
F1 = 20.3	NODE 1 = 0.11
F2 = 2.3	NODE 2 = 2.2
1i = 0.35	NODE 3 = 1.0
i2 = 1.6	
23 = 2.6	
3G = 10.3	

Figure 3. Nodal configuration and table of estimated values.

and the nodal time constant is given by

$$\tau_2 = R_{n2} C_2$$

Nodes of the model that do not provide an energy storage function are also absent the associated time constant. Thus the temperature at the internal node shown at the interface between the tip and fin of the present model (node i in Fig. 3) is expressed in terms of the temperature of the surrounding nodes with only thermal resistances as parameters.

A heat balance at each of the remaining nodes yields relationships similar to those given above, so sufficient information is available to determine each nodal temperature as a function of time. Initially, the system is assumed to be at thermal equilibrium with the environment so that the nodal temperatures are all equal to the ambient value. With the firing of the rocket motor this equilibrium is disturbed and the two recovery temperatures provide inputs to the ensuing heat transfer process. In preliminary studies the Digital Simulation Language (DSL) has been used to automatically accomplish the repeated integration steps required to determine the thermal response of those nodes possessing storage capacities.

The calculation method, together with preliminary results, are described in later sections. Before this, however, it is necessary to estimate the driving functions of the entire process -- the thermal inputs at the tip and fin surfaces. This is the subject of the next chapter.

IV. ESTIMATES OF SURFACE HEAT TRANSFER RATES

As described in the previous section, the forcing functions of particular interest are those due to heating at the vane tip and along the downstream surface of the vane. (The cooling effects of radiation and ablation, both clearly important in the actual situation, are omitted from discussion for the time being.) Most of the heat transfer computations outlined below are derived from the analytical methods suggested in the works edited by C.C. Lin [12] and in the AGARD Monograph authored by Ziebland and Parkinson [10].

A particular feature of these high speed flows is the large differences in temperature that the gas experiences in decelerating near the body surface. In such cases it is necessary to account for the temperature dependency of gas properties. A most-useful simplification for this purpose is that proposed by Diessler and others [12, p.304] in which the Prandtl number and specific heat are considered to be constant inasmuch as their variations with temperature are of a lower order of magnitude than those of the other gas properties (viscosity and thermal conductivity). Thus, with this assumption, the quantity Pr/c_p = constant and a separate estimate of the gas viscosity leads to the thermal conductivity for a given Prandtl number and specific heat.

For the rough calculations used in this study, the Prandtl number has been estimated using the Eucken formula [2, p.139], $Pr = 4k/(9k-5)$, where k is the ratio of specific heats. With the gas constant, R_g, the constant-pressure

specific heat is given by $c_p = R_g k/(k-1)$.

In this work, the standard Sutherland-type formula has been adopted for determining viscosity:

$$\frac{\mu}{\mu_{ref}} = \left(\frac{T}{T_{ref}}\right)^n$$

Following the recommendation of [2, p.9], a value of n = 0.7 has been used. In addition, the reference viscosity has been taken to be $\mu_{ref} = 4.0 \times 10^{-5}$ N-s/m^2 at $T_{ref} = 1000$ K.

Stagnation Point Heat Transfer

In the analysis of stagnation point heating, the solution to the boundary layer equation requires an estimate of the local fluid acceleration in the vicinity of that point. In the case of supersonic flow, this can be approximated upon the assumption that Newtonian flow prevails between the bow wave

bow wave and the body and, (see van Driest [1, p.366]),

$$\beta = (du_e/dx)_{x=0} = (U/D)\left[\delta(P_\infty/P_{oy})(T_{o\infty}/T_\infty)\right]^{0.5}$$

Here the subscript (∞) refers to freestream conditions, (o) denotes stagnation conditions, and (y) is for conditions downstream of the normal shock. The pressure and temperature ratios in the above expressions are known functions of the freestream Mach number.

With β thus defined, the Stanton number may be computed from the following:

$$St_o = 0.57\ (\beta D/U)^{0.5} Pr_o^{-0.6}\ Re_o^{-0.5}$$

Turbulent Boundary Layer Convection

In high speed compressible flows, the analysis of thermal processes is complicated by the fact that considerable compression and viscous dissipation follow from the decelerations occuring in the boundary layer. This leads to temperatures within the boundary layer that are in excess of that of the freestream, and the driving temperature for heat transfer is the so-called recovery temperature, T_R. Thus a recovery factor is defined as follows:

$$r = \frac{T_R - T_\infty}{T_o - T_\infty}$$

Fortunately, it has been found by many investigators that the recovery factor may be related to the Prandtl number in a simple way that is adequate for most purposes. For a turbulent boundary layer (assumed here), the relationship is $r = Pr^{1/3}$.

A more-difficult problem arises from the dependency of gas properties upon temperature since in most cases the appropriate reference temperature for this calculation depends upon the wall temperature. This, in turn, depends upon the reference temperature. The reference temperature is typically defined as [2]

$$T_{ref} = 0.5\ T_{wall} + 0.28\ T_\infty + 0.22\ T_R$$

The present calculations are based upon the assumption that the wall temperature is adequately represented for this purpose by the mean of the recovery and ambient temperatures. (An evaluation of the validity of this assumption requires

an iterative time-dependent calculation. In the system identification work to be described, however, the convective resistance is treated as a parameter to be identified. Thus the experimental data lead to the deduction of the "effective" film coefficient and the detailed analyses described in this section may not be necessary for design purposes.)

Given that the reference temperature for gas properties is adequately described, the gas viscosity and thermal conductivity may be estimated as above. The Stanton number for turbulent compressible flow is then given by [2]:

$$St = 0.0296\ Pr^{-0.67}\ Re^{-0.2}$$

From the expressions given above for the Stanton numbers, Nusselt numbers and thermal resistances can be calculated for the model components affected by stagnation and boundary layer heat transfer processes. It should be noted that the thermal resistances are scale-dependent: stagnation point thermal resistance decreases as $(scale)^{-1.5}$, and turbulent boundary layer thermal resistance is propportional to $(scale)^{-1.2}$. The simulations conducted in this study have been of a 1/4-scale vane in order to provide a comparison with available NWC test data.

Input Modeling

The information necessary to provide values for the thermal resistance includes the freestream characteristics at the location of the jet vane -- Mach number, stagnation temperature, and stagnation pressure. The concept of the present model is that these quantities are determined from

the ballistic characteristics of the rocket motor. Accordingly, inputs required for the simulation include the motor chamber pressure, thrust, and characteristic velocity, and the discharge coefficient and pressure ratio of the nozzle. In addition, necessary propellant gas properties include the ratio of specific heats and the gas molecular weight or gas constant. Experimental values are preferred, to the extent that they are available, but a considerable body of theory exists if analytical estimates are necessary.

From these quantities, the stagnation temperature may be calculated as follows:

$$T_o = [C_d \Gamma c^*]^2/R_g$$

where:

C_d = nozzle discharge coefficient (.934)

Γ = $[k(2/k+1)^{(k+1)/(k-1)}]^{0.5}$ (0.65)

c^* = characteristic velocity (1512 m/s)

R_g = gas constant (318.5 m^2/s^2-K)

k = ratio of specific heats (1.21)

The numbers given in parentheses are those presently in use, and lead to a stagnation temperature of 2650 K.

From the motor nozzle pressure ratio Mach number at the exit (assumed to be that at the vane) is computed from

$$M_e^2 = [2/(k-1)] [(P_{oe}/P_e)^{(k-1)/k} - 1]$$

and selecting a nozzle pressure ratio of P_{oe}/P_e = 186, this expression gives M_e = 3.75. It is important to note that the motor chamber pressure must also be provided because the heat transfer calculations for the vane require the density

and hence the pressure in the freestream at the vane location -- in the calculations presented here, the value of $P_{0\infty}$ = 15.76 MPa has been used.

For ease of reference, the following table of values describes the heat transfer quantities obtained from the inputs and computed quantities described above.

	Stagnation Point	Turbulent Boundary Layer
Stanton number	8.53×10^{-3}	3.01×10^{-3}
Nusselt number	43.1	438
Film coefficient, W/m^2-K	6.46×10^{3}	2.25×10^{3}
Thermal resistance, K/W	5.69	0.634

V. SIMULATION RESULTS

The model and governing equations, described above, have been coded in the Digital Simulation Language (DSL). This IBM software product is a FORTRAN-based language with the particular advantage that a wide variety of integration subroutines are imbedded and directly available to the user. Such integrations are necessary at each of the energy storage nodes, and for this purpose a 5-th order Runge-Kutta method incorporating a variable step size was selected. In addition to the vane conduction model described above, the code incorporates energy flow calculations in order to verify that the model does indeed account for the disposition of all heat transferred to or from the vane, as well as that

stored at the various nodes.

The simulation code has been written so that the driving input is the thrust of the rocket motor, as provided by test data. In the case reported here, the point-by-point thrust vs. time measurements are approximated by a ramp input from 0 to 2335 N (525 lb) in a period of 0.5s, held at this level for 2.5s, and ramped back to zero thrust in a further period of 0.5s. Although the actual thrust data points could be used, the ramp-up/ramp-down closely approximates the thrust schedule and provides a useful input for evaluating the sensitivity of the thermal response of the vane to various parameters of the model.

An important aspect of the physical event of rocket firing is that the convective resistances to vane heat transfer (at the stagnation point and in the boundary layer) are coupled to the presence or absence of flow past the vane. Thus these resistances are initially very large, decrease rapidly to plateau values as the motor reaches full thrust, and increase again during burnout. This behavior has been modeled by postulating that the film coefficients begin and end at 1% of the full-flow values and follow the ramp-up, plateau, ramp-down profile of the thrust schedule.

For comparison with the simulation results, the vane temperature data were likewise converted to a continuous record by means of the transfer function furnished by NWC [13]. This transfer function, which was deduced from the test data, closely approaches the actual measurements and is

given as

$$\frac{T_3}{\text{THRUST}} = \frac{8}{(1.233s+1)(50.76s+1)}$$

(In this expression, thrust in Newtons gives a temperature response in degrees Fahrenheit above ambient.)

Vane Thermal Response

Figure 4 shows the computed vane temperature history using "current best estimates" of the problem parameters described previously. This figure shows that the predicted temperature-time history at the reference shaft node is well in excess of that obtained in the tests.

In the model as it is presently configured, the quantities encumbered by the greatest amount of uncertainty are those associated with the boundaries of the thermal system -- the convective inputs and the conductive cooling of the vane by the thermal sink effect of the mount. Some preliminary experimentation with the simulation has led to the insight that the chief control over the maximum shaft temperature is the mount thermal resistance. On the other hand, the dynamic temperature rise is mainly affected by the convective thermal resistances acting at the vane surface. These observations lead to the premise that the effective time constants for these two processes are widely separated -- a clue to which is given in the previous transfer-function model.

Adjustment of these factors leads results of the sort shown in Fig. 5. which illustrates the sensitivity of the

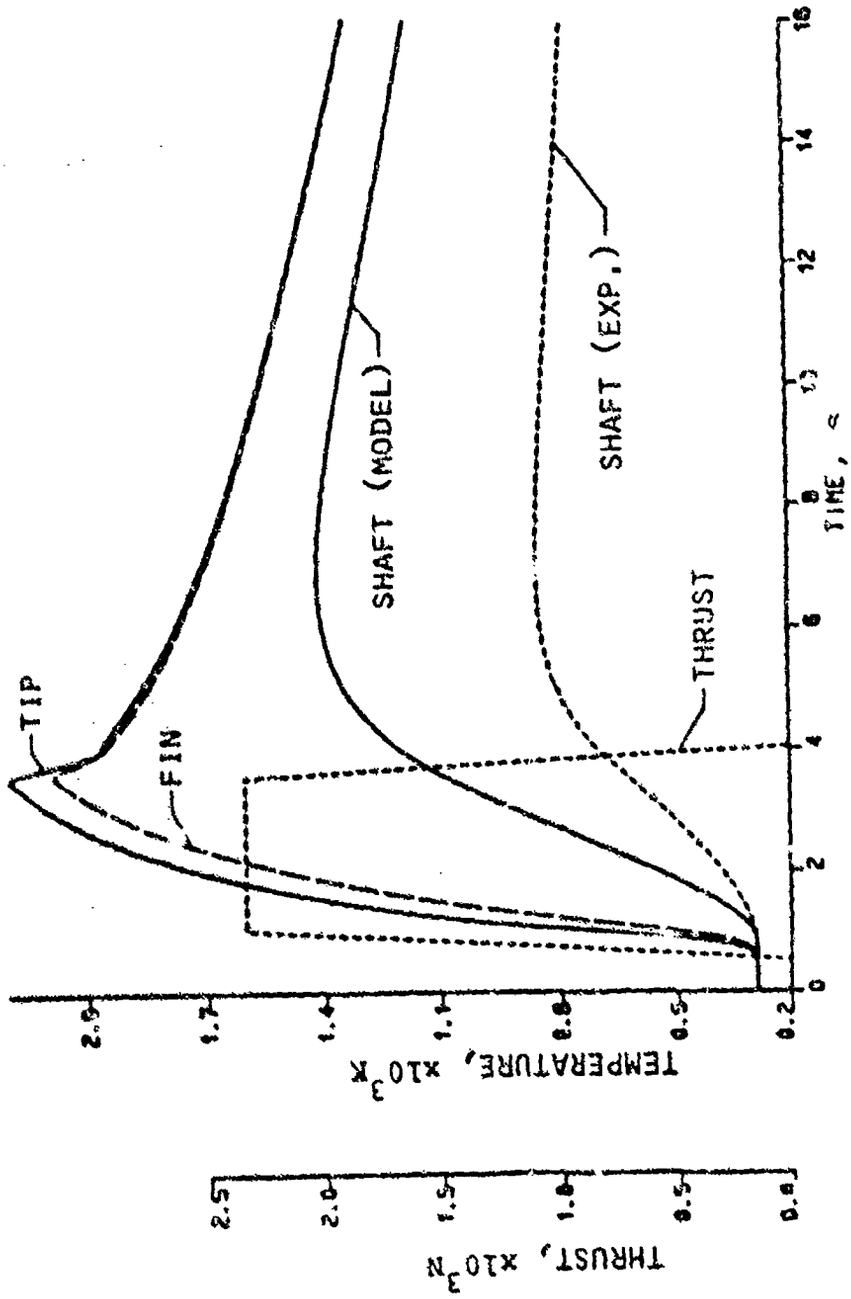

Figure 4. Vane thermal response.

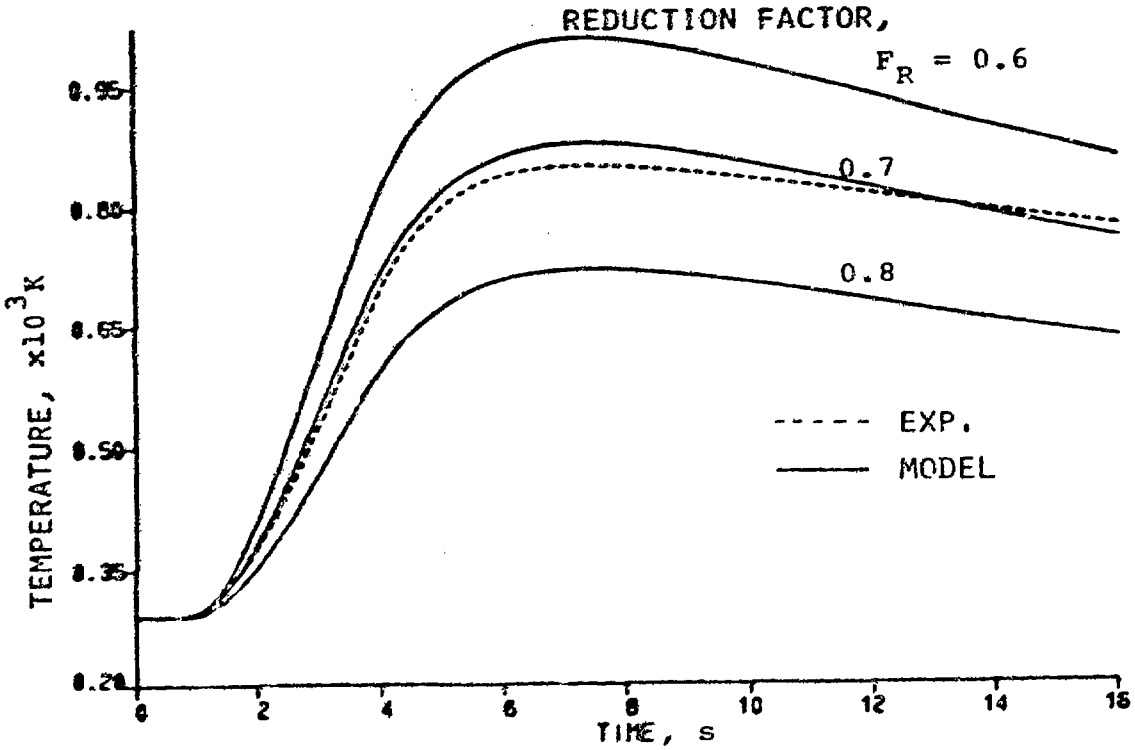

Figure 5. Shaft temperature histories, various R_F.

shaft temperature response to the convective film coefficients. It will be seen from this figure that in order to obtain reasonable agreement between theory and experiment it is necessary to reduce these coefficients (with corresponding increases in the respective thermal resistances) by a factor on the order of 60% to 80% -- the ratio F_R in Fig. 5. The need for this offset is largely attributable to omission of the cooling effects of radiation and ablation. It is apparent, however, that the model is capable of reproducing the main transient features (time constants) of the vane thermal response.

Figure 6 illustrates the sort of agreement with test data that is achievable using the present model. To achieve the results shown in Figs. 5 and 6, result, a mount thermal resistance of R_{3G} = 10.3 K/W was used -- a value not inconsistent with the mass and configuration of the mount. Whether or not the reduction factor of 72% is consistent with the effect of radiative and ablative cooling is yet to be determined. In any case, it is noteworthy that the agreement illustrated in Fig. 6 is attainable by means of a single constant factor.

In addition to providing the framework of a working computational code, the results of the simulation indicate that it may be feasible to predict the bulk thermal behavior of selected critical elements of the jet vane. In order to obtain these preliminary results, no particular attention has been paid to the precision with which the boundary ther-

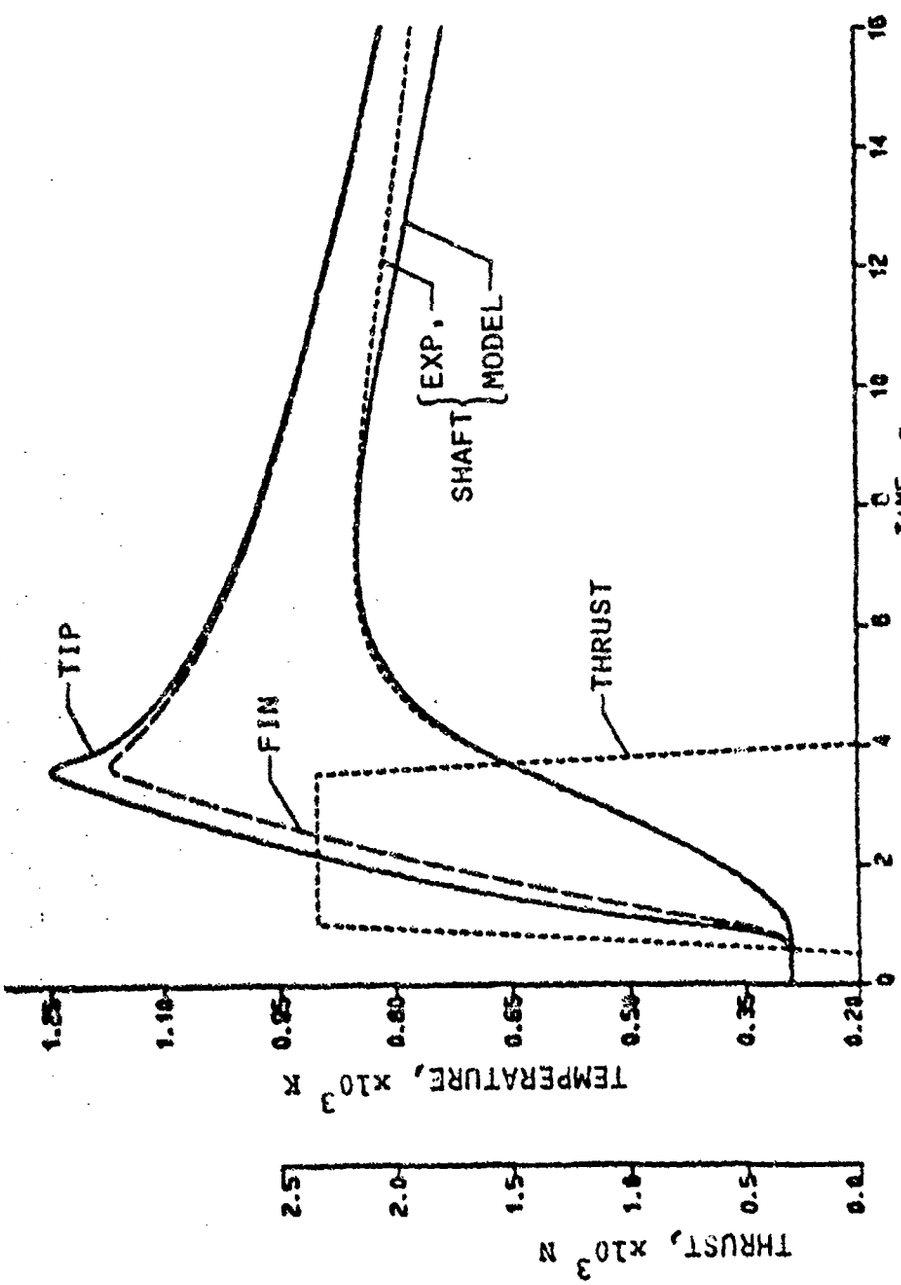

Figure 6. Temperature vs. time, $F_R = 0.72$.

mal resistances are calculated. For the purposes of this work, the simplicity of the model gives some encouragement that it may be adaptable to the deductive or system-identification mode of analysis. Preliminary results, reported in subsequent sections of this report, indicate that this is in deed the case.

VI. STATE SPACE MODEL FORMULATION

The results presented thusfar have been obtained from a sequential integration of the energy balance relationships at each calculation node, and Eq. (2) illustrates the form in which these relationships have been cast in the DSL program for purposes of simulation. If the physical quantities (resistances and capacitances) appearing in the governing system of equations are truly constant, then the system is linear and the efficiency of a state space formulation may be brought to bear. The matrix formats that characterize the state space formulation are particularly useful in providing a systematic presentation of the mathematical model.

In addition, the following results have been obtained using the personal computer version of the software package called "MATRIXx" (product of Integrated Systems Incorporated, Palo Alto, Calif.). Incorporated in MATRIXx is a vast variety of matrix manipulation schemes that are often found to be essential in the modeling and simulation of dynamic systems (particularly control systems). Included are means for conversion from continuous to discrete systems and for

transformation of systems from state space to transfer function models and vice-versa. The system identification capabilities of MATRIXx, essential to the goals of this study, are discussed in a subsequent chapter.

Mathematical relationships are expressed in state space form by arranging them such that the highest order derivatives of the dependent variables (the temperatures at the various nodes, in this case) are given as linear functions of the lower order derivatives. For node 2, for instance, Eq. (1) may be written

$$\dot{T}_2 = -\frac{T_2}{C_2}\left(\frac{1}{R_{F2}} + \frac{1}{R_{i2}} + \frac{1}{R_{23}}\right) + \frac{T_i}{C_2 R_{i2}} + \frac{T_3}{C_2 R_{23}} + \frac{T_{R2}}{C_2 R_{F2}} \qquad (3)$$

Referring to Fig. 3, the corresponding relationships for nodes 1 and 3 are obtained:

$$\dot{T}_1 = -\frac{T_1}{C_1}\left(\frac{1}{R_{F1}} + \frac{1}{R_{1i}}\right) + \frac{T_i}{C_1 R_{1i}} + \frac{T_{R1}}{C_1 R_{F1}} \qquad (4)$$

$$\dot{T}_3 = -\frac{T_3}{C_3}\left(\frac{1}{R_{23}} + \frac{1}{R_{3G}}\right) + \frac{T_2}{C_3 R_{23}} + \frac{T_G}{C_3 R_{3G}} \qquad (5)$$

The internal node designated (i) in Fig. 3, which was included to allow separate estimation of the tip and vane resistances, is not a storage node and, as previously noted, energy balance for this node does not include a rate term:

$$\frac{T_1 - T_i}{R_{1i}} = \frac{T_i - T_2}{R_{i2}} \qquad (6)$$

Equation (6) may be solved for T_i and Eqs. (3) and (4) may be used to obtain an expression for its rate of change in the format of Eqs. (3)-(5). This would lead to a four-state

formulation for the four node temperatures. For efficiency of computation, however, it seems good practice to eliminate such non-storage nodes from consideration -- temperatures at such nodes can always be calculated from algebraic expressions, such as Eq. (6), involving the temperatures at adjacent nodes. Using Eq. (6) to eliminate T_1 from Eqs. (3) and (4) gives the following 3-state set:

$$\dot{T}_1 = -\frac{T_1}{C_1}\left(\frac{1}{R_{F1}} + \frac{1}{R_{12}}\right) + \frac{T_2}{C_1}\frac{1}{R_{12}} + \frac{T_{R1}}{C_1}\frac{1}{R_{F1}} \tag{7}$$

$$\dot{T}_2 = \frac{T_1}{C_2}\frac{1}{R_{12}} - \frac{T_2}{C_2}\left(\frac{1}{R_{F2}} + \frac{1}{R_{12}} + \frac{1}{R_{23}}\right) + \frac{T_3}{C_2 R_{23}} + \frac{T_{R2}}{C_2}\frac{1}{R_{F2}} \tag{8}$$

$$\dot{T}_3 = \frac{T_2}{C_3}\frac{1}{R_{23}} - \frac{T_3}{C_3}\left(\frac{1}{R_{23}} + \frac{1}{R_{3G}}\right) + \frac{T_G}{C_3}\frac{1}{R_{3G}} \tag{9}$$

where $R_{12} = R_{i1} + R_{i2}$.

Arranged in such a fashion, it is apparent that the nodal expressions possess a certain amount of symmetry. Each of the coefficients of temperature on the righthand sides of Eqs. (7)-(9) have the dimension of inverse time and, in fact, the RC products are representations of the time constants describing the energy transport processes occuring at and around the nodes. To further illustrate this formal arrangement, it is useful to define the following parameters (inverse time constants):

$$a_{11}=-(a_{12}+a_{13}+b_{11}),\quad a_{12}=1/C_1R_{12},\quad a_{13}=0$$

$$a_{21}=1/C_2R_{12},\quad a_{22}=-(a_{21}+a_{23}+b_{22}),\quad a_{23}=1/C_2R_{23} \tag{10}$$

$$a_{31}=0,\quad a_{32}=1\backslash C_3R_{23},\quad a_{33}=-(a_{31}+a_{32}+b_{33})$$

where

$$b_{11} = 1/C_1R_{F1} \ , \ b_{22} = 1/C_2R_{F2} \ , \ b_{33} = 1/C_3R_{3G}$$

With these definitions, Eqs. (7)-(9) may be written

$$\dot{\underline{T}} = \underline{A}\,\underline{T} + \underline{B}\,\underline{U} \qquad (11)$$

where the "state" consists of the n = 3 nodal temperatures:

$$\underline{T} = (T_1 \quad T_2 \quad T_3)' \ ,$$

the "input" vector contains the m = 3 boundary temperatures:

$$\underline{U} = (T_{R1} \quad T_{R2} \quad T_G)' \ ,$$

and the nxn matrix $\underline{A}$ and the nxm matrix $\underline{B}$ are given by

$$\underline{A} = \begin{bmatrix} a_{11} & a_{12} & a_{13} \\ a_{21} & a_{22} & a_{23} \\ a_{31} & a_{32} & a_{33} \end{bmatrix} \ , \quad \underline{B} = \begin{bmatrix} b_{11} & 0 & 0 \\ 0 & b_{22} & 0 \\ 0 & 0 & b_{33} \end{bmatrix}$$

Equation (11) is expressed in the state-space form familiar to the analysis of controls systems, and if the vector of input temperatures $\underline{U}$ are specified the time histories of the nodal temperatures are easily obtained.

Because the "ground" temperature T_G is a specified constant in this model (in the case at hand it is 290K) the calculation may be simplified by referring all temperatures to ground. This has the effect of removing the ground temperature as an input (it is zero relative to itself) and the input vector becomes $\underline{U} = (T_{r1} \quad T_{r2})'$. With only the recovery temperatures as inputs (m = 2) the last column in the input coefficient matrix $\underline{B}$ is redundant and must be deleted.

The three nodal temperatures are "outputs," in a control systems sense, and the usual output relationship may be written as

$$\underline{y} = \underline{C}\,\underline{T} + \underline{D}\,\underline{U}$$

where $\underline{C}$ is a 3x3 identity matrix and $\underline{D}$ is a 3x2 null matrix. As a final step prior to simulation, the four matrices may be combined into a single partitioned matrix, $\underline{S}$, containing the four submatrices $\underline{A}$, $\underline{B}$, $\underline{C}$, and $\underline{D}$. This is particularly useful when dealing with the MATRIXx software. Thus

$$\underline{S} = \left[\begin{array}{c|c} \underline{A} & \underline{B} \\ \hline \underline{C} & \underline{D} \end{array}\right], \text{ or}$$

$$\underline{S} = \begin{bmatrix} a_{11} & a_{12} & a_{13} & b_{11} & 0 \\ a_{21} & a_{22} & a_{23} & 0 & b_{22} \\ a_{31} & a_{32} & a_{33} & 0 & 0 \\ 1 & 0 & 0 & 0 & 0 \\ 0 & 1 & 0 & 0 & 0 \\ 0 & 0 & 1 & 0 & 0 \end{bmatrix} \tag{12}$$

In this formulation the thermal characteristics of the system are specified in the $\underline{A}$ matrix and the input resistances are found in the elements making up the $\underline{B}$ matrix. Note that the diagonal elements of the $\underline{A}$ matrix are the negative inverses of the characteristic time constants for the thermal response of each of the nodes. As defined in Eq. (10), these diagonal elements are sums of the values on the corresponding row, including the input matrix. This relationship expresses the conservation of energy embodied in the analysis and the diagonal elements cannot be independently varied without violating this principle. This is an important constraint when system identification procedures are applied to the system.

The generality of the formulation is apparent, and there would be no particular difficulty in adding storage nodes to the model in order to obtain a more-detailed view of the temperature distribution within the vane. Such refinement at this point seems unwarranted, however, since little information is available to allow a concomittant refinement of the distribution of the thermal inputs. In fact, the present model would not be drastically affected if the stagnation point and boundary layer heat transfer were combined into a single input, thus reducing the model to a two-state system.

SIMULATION IN STATE SPACE

Figure 3 includes a table of the thermal resistances and nodal capacitances that have been estimated for the problem at hand. (In estimating the "effective" input resistances given in Fig. 3, the calculated heat transfer coefficients have been reduced by the 72% factor leading to the results described in the previous chapter.) When these values are incorporated into the present analysis, the $\underline{A}$ and $\underline{B}$ matrices take the following values:

$$\underline{A} = \begin{bmatrix} -3.15 & 4.7 & 0 \\ 0.23 & -0.61 & 0.18 \\ 0 & 0.38 & -0.48 \end{bmatrix} \qquad \underline{B} = \begin{bmatrix} 0.45 & 0 \\ 0 & 0.20 \\ 0 & 0 \end{bmatrix} \tag{13}$$

For the tip node the input temperature is the stagnation temperature (2650K) and for the vane the recovery temperature calculated by the methods of Ch. IV is 2550K (very nearly the same as the stagnation temperature in this high-

speed compressible flow). When referred to an ambient temperature of 290K, the appropriate input values for temperature are

$$T_{R1} = 236^{\circ}K \quad \text{and} \quad T_{R2} = 226^{\circ}K$$

Although the thrust was used as the fundamental input for the simulations previously described, these temperatures may be assumed to follow an input schedule that is more-or-less synchronous with the thrust. Accordingly, in the simulations that follow the recovery temperatures have been given the same ramp-up, plateau (at the values given above), and ramp-down contour that is described in Ch. V.

Linear Time-Invariant (LTI) Model

With the model matrices values given in Eq. (13) and the scheduled input temperatures described above, simulation of the vane thermal response is accomplished using the MATRIXx LSIM command [14, p.10-6]. In this case, the syntax is

$$[T, \underline{Y}] = \text{LSIM}(\underline{S}, NS, \underline{U}, DELTAT)$$

where $\underline{S}$ is the system matrix formed as in Eq. (12) and incorporating the values given in Eq. (13); NS is the number of states (NS = 3 -- the three nodal temperatures); $\underline{U}$ is the input array, in this case expressing the scheduled input temperatures; and DELTAT is the specified time increment between steps in the $\underline{U}$ array. In all simulation cases described herein, a time increment of 0.1s has been used for a duration of 15s. Thus the time vector has dimensions 151x1 and the $\underline{U}$ array is 151x2 for the two inputs.

Figure 7 shows the results of the simulation assuming

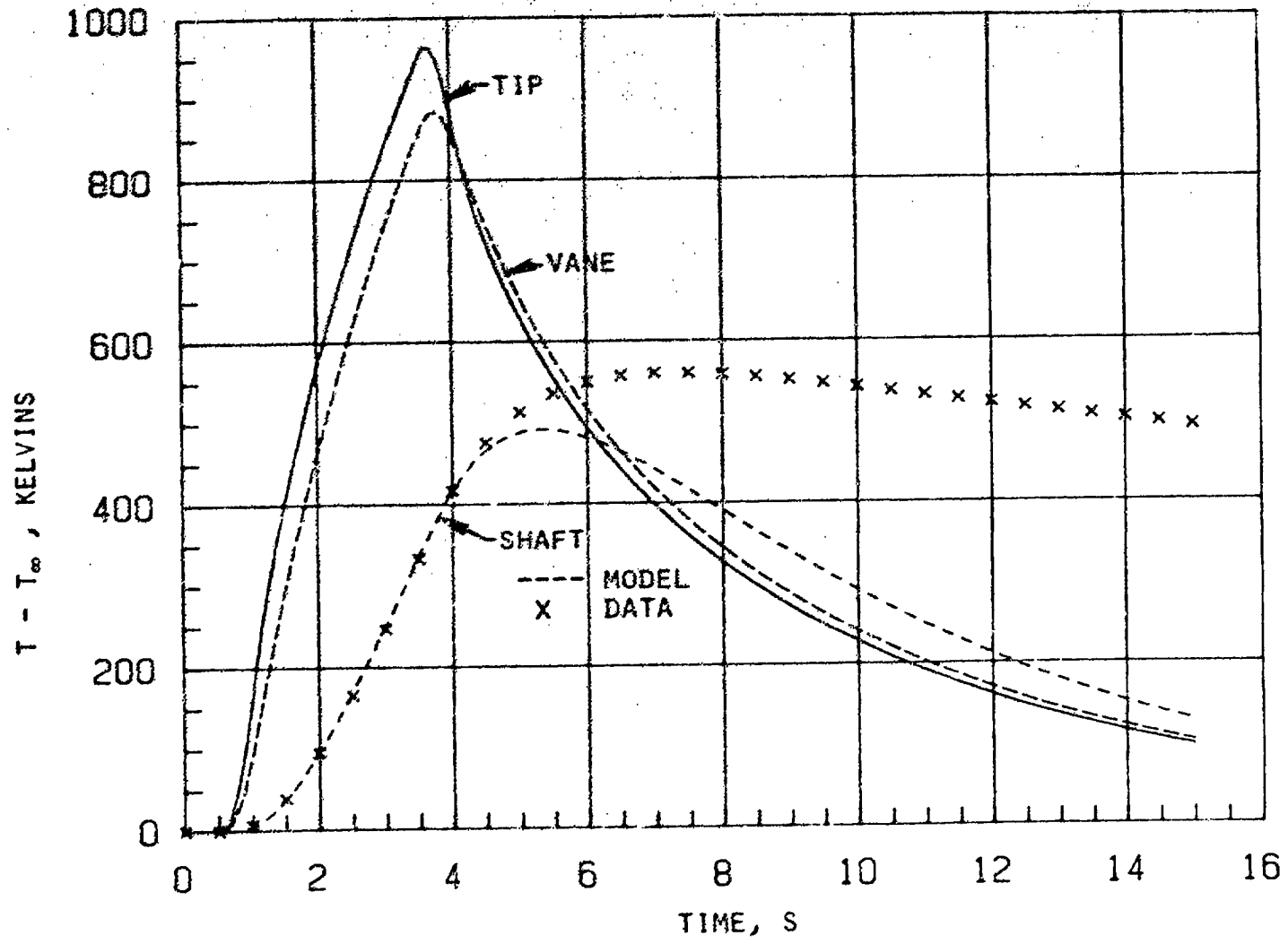

Figure 7. Vane thermal response -- LTI baseline simulation.

that the elements of the A and B matrices are constant with time. As expected, the results are unsatisfactory because the linear time-invariant (LTI) assumption does not account for the variation of the heat transfer coefficients with time. In other words, the elements of the B matrix and the diagonal elements of the A matrix must be calculated at each time step in the simulation.

Linear Time-Variant (LTV) Model

With MATRIXx, the accomodation of time-varying parameters may be relatively easily achieved by using the SYSTEM BUILD capability. SYSTEM BUILD provides an interactive, menu-driven graphical environment for building, modifying, and editing computer simulation models. Any combination of linear, non-linear, continuous-time, discrete-time, or multi-rate models that describe a system may be constructed from a library of basic building blocks. Systems may be modeled by dividing them into individual components with each component being described by a specific type of functional block. Super-blocks can be used to represent assemblies of individual blocks and the heirarchical design provides an organized representation of the physical system that is modeled.

In SYSTEM BUILD, any super-block or set of nested super-blocks can be simulated, linearized, and analyzed. No user coding is necessary (although it is allowed), and SYSTEM BUILD can be driven by user-defined command procedures that automatically build or modify system models. All of

this capability is available for PC hardware (which has been used thusfar in this study) and the net effect of the SYSTEM BUILD capability is that the user may concentrate efforts on design, analysis, and simulation in an efficient graphical environment.

The SYSTEM BUILD Model. In this study, the vane thermal behavior has been modeled by means of seven super-blocks named as follows:

NOD1IN, NOD2IN, NOD3IN

NODE1, NODE2, NODE3

VANE5

The appendix provides illustrations of these super-blocks, and a brief discussion will be provided here.

The first three blocks are compute the parameters necessary for the state equation. The input to both NOD1IN and NOD2IN is the ramp-up, plateau, ramp-down schedule previously described, but with a plateau value of unity. In NOD1IN, for example, this input is multiplied by T_{R1} and b_{11} as gains to form the time-varying element in the first row of the input coefficient array $\underline{B}$. Also in NOD1IN, the quantity a_{12} is generated by means of the step function and this, in turn, is used to form $-a_{11} = a_{12} * b_{11}$ as given in Eq. (10). The outputs of NOD1IN are $-a_{11}$, $b_{11}T_{R1}$, and a_{12}. NOD2IN and NOD3IN are similar in function, with the exception that NOD3IN does not require the time-varying input.

The first three super-blocks listed above are elements of the second three, respectively. In NODE1, for example,

the external input T_2 is combined with the outputs of NOD1IN to form the quantity $a_{11}T_1 + a_{12}T_2 + b_{11}T_{R1} = \dot{T}_1$. An integration is also within NODE1 to obtain T_1 from $\dot{T}_1$. T_1 is the output of the NODE1 super-block and, in a similar way, NODE2 and NODE3 provide outputs T_2 and T_3.

Super-block VANE5 "wires" NODE1, NODE2, and NODE3 together in order to provide simultaneous solution for the three nodal temperatures. In VANE5 (see appendix), NODE1 receives the dual ramp input and T_2 while generating T_1; NODE2 receives the dual ramp input, T_1, and T_3 while generating T_2; and NODE3 receives T_2 and outputs T_3.

To execute the SYSTEM BUILD model, the program is first checked by means of the ANALYZE command [15]. Following this, one of six integration methods may be selected from the menu provided. The results described here have been obtained with a variable-step Kutta-Merson scheme which is an explicit fourth-order method that employs the largest time step possible while remaining within error tolerances (maximum step size is the time increment specified for the simulation).

Simulation is achieved by executing the SYSTEM BUILD command SIM, as in "$\underline{Y}$ = SIM(T,$\underline{U}$)", where the time vector T and the input $\underline{U}$ must be provided. In the case at hand, T is the 151x1 vector containing 15 seconds of 0.1-second steps and $\underline{U}$ is the 151x2 array exhibiting the ramp-up, unity plateau, ramp down schedule previously described.

Figure 8 shows the results of simulation using the

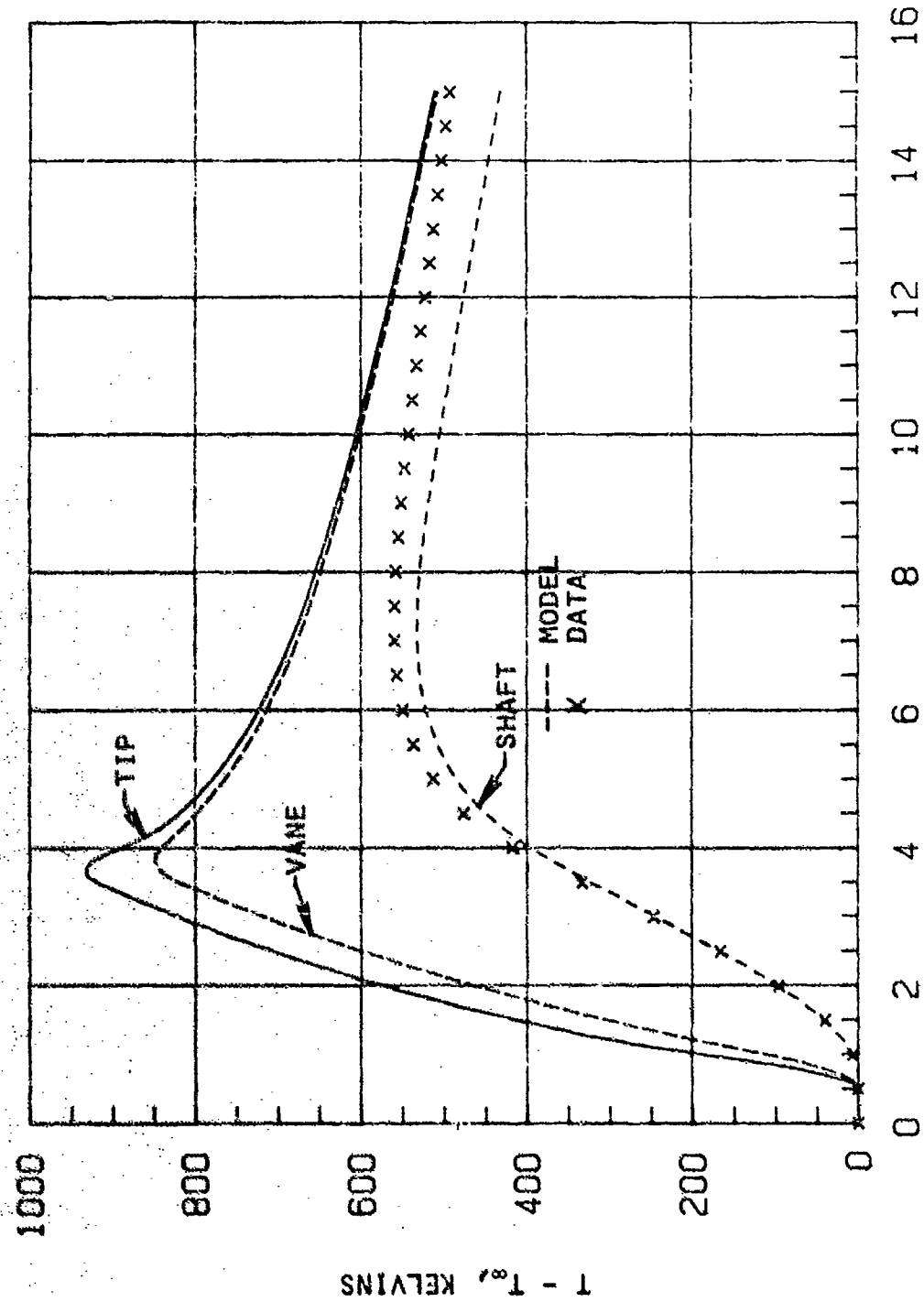

Figure 8. Vane thermal response -- LTV baseline simulation.

SYSTEM BUILD model to provide linear time-variant (LTV) behavior of the vane heat transfer coefficients. In this figure the improvements attained with the SYSTEM BUILD LTV model are apparent. With the model now cast in this format it is possible to take the system identification approach that has been the ultimate goal of this study.

VIII. PARAMETRIC SYSTEM IDENTIFICATION

The philosophy of parameteric system identification (PSI) is to use measured response data to "massage" the parameters of a system model such that simulation results match those of experiments. Some of this has already been accomplished by the manual variation of parameters described in Ch. V, but PSI will now be used to complete this process in a systematic way.

In the problem at hand, it is reckoned that the most uncertain parameter values are those associated with the heat transfer processes at the vane surface and the thermal sink effects of the vane mount. The vane temperature to be matched is that of the shaft (T_3), and although the stagnation heat transfer process at the vane tip has been modeled this provides relatively little heat flux into the vane and is therefore of secondary importance as far as the thermal response at the shaft is concerned.

Thus the results described here have been obtained by a two-parameter variation involving b_{22} and a_{33}. It is to be recalled that the variation of b_{22} will also require a

change in a_{22} in accordance with the energy balance, and that this is accomodated in the SYSTEM BUILD model. In addition, the value of a_{33} has within it b_{33} which is not used in the simulation since the relative ground temperature is zero. Nevertheless, a knowledge of a_{33} will lead to the appropriate value of b_{33} since $b_{33} = -a_{33} - a_{32}$ as given in Eq. (10).

The MATRIXx/PC family includes a variety of capabilities that provide for data analysis, parametric and non-parmetric system identification, and digital filtering. In this work, PSI is achieved by using a scheme known as "maximum likelihood estimation" (MLE) [16]. As its name implies, MLE maximizes the likelihood of the parameter estimates given the observations (in this case, the measured transient response of T_3). MLE operates on an entire time history (rather than one sample at a time) and is applicable to multiple-input/multiple-output (MIMO) systems such as that under analysis here.

The command that executes the MATRIXx version of the MLE procedure is MAXLIKE [17], with the following syntax:

[YHAT,P] = MAXLIKE(U,T3,P0,'VBM2',NIT)

Items to be provided by the user are U, containing the time vector and array of input coefficients; T3, the vector of observed values that are the standards for comparison; P0, the vector of initial estimates for the parameters to be varied;'VBM2', a user-supplied command file that creates the values of T3 based upon U and the current values of P; and

NIT, the specified number of iterations to be performed.

The results of MAXLIKE are YHAT, the system response using current values of the parameters; P, which contains these current values; and RSS which is the sum of the squares of the differences between the measured and predicted values at each time step -- RSS = sum(T3 - YHAT)^2.

As has been shown, the LTV nature of the vane heat transfer problem requires the use of SYSTEM BUILD. Thus, in the problem at hand, the command file 'VBM2' reads as follows:

```
BUILD,EDIT,NOD2IN,0,EXAMINE,2,NEW,P(1),DONE,TOP,...
      EDIT,NOD3IN,0,EXAMINE,3,NEW,P(2),DONE,TOP,...
      ANALYZE,VANE5
Y3=SIM(U(:,1),U(:,2:3));
YHAT=Y3(:,3);
RETURN
```

Although this language may not be familiar to the reader, it may be possible to deduce that in the SYSTEM BUILD lexicon these instructions sequentially update P(1) (= b_{22}) which is in position 2 of super-block NOD2IN and P(2) (= a_{33}) which is in position 3 of super-block NOD3IN. Y3 is the name given to the three-temperature array obtained from simulation using the current parameter values, P(1) and p(2), with YHAT (= T_3) contained in third column. It should be noted that in each iteration the MAXLIKE procedure executes 'VBM2' at once for each parameter value under consideration.

Figure 9 is the result of a PSI run of three iterations

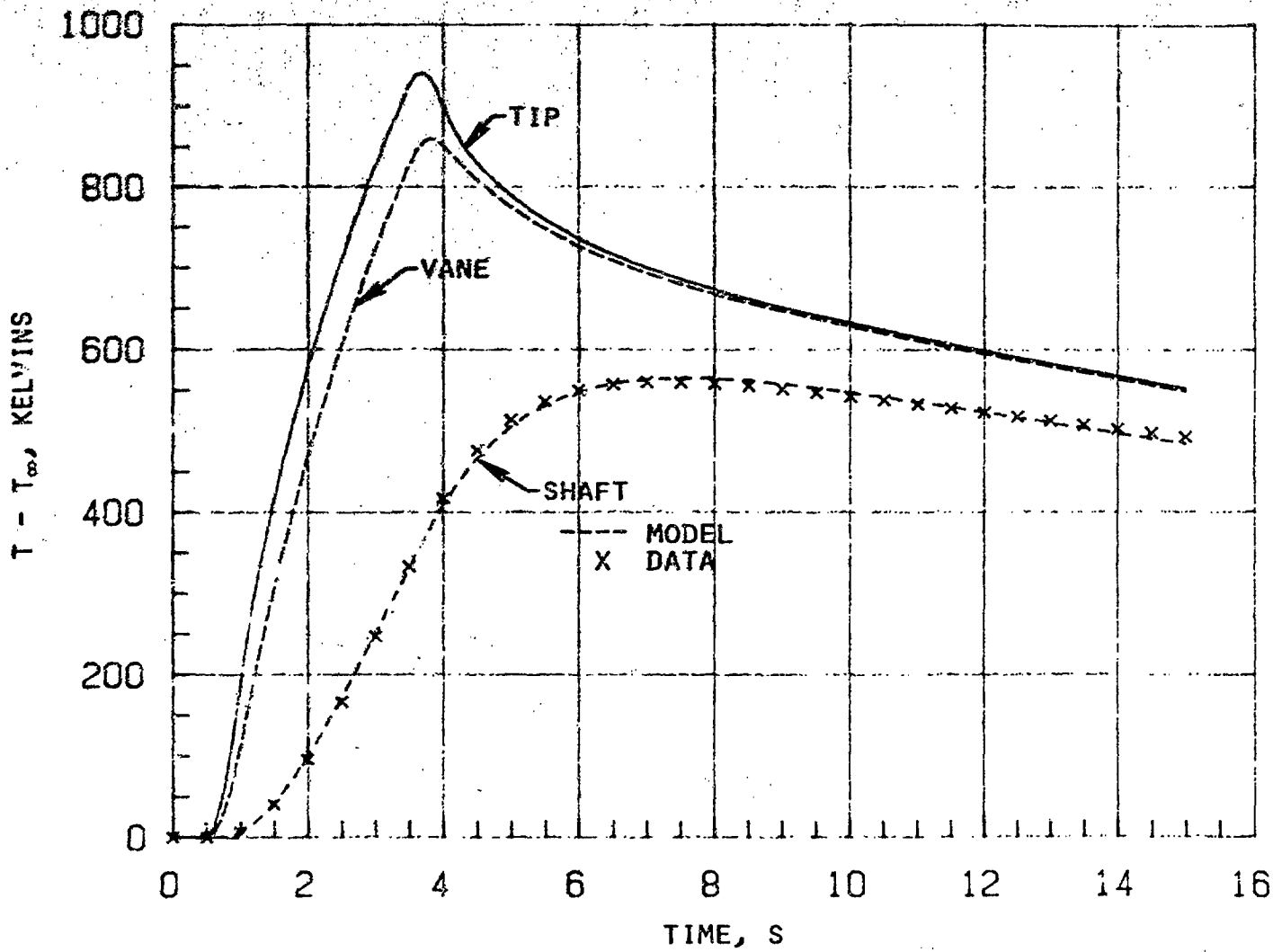

Figure 9. Vane thermal response -- LTV simulation after system identification.

using initial parameter values given previously (b_{22} = 0.20 and a_{33} = -0.48). The "maximum likelihood" values obtained through the use of PSI, and giving the results shown in Fig. 9, are b_{22} = 0.2027 and a_{33} = -0.4565. The value of the residual associated with these results is RSS = 59.4. (This is a very small value, bearing in mind that it is a sum of 151 squared temperature differences.)

Discussion of the PSI Results

As was done in Ch. V, the experimental shaft temperature data (shown as x's in Figs. 7-9) have been obtained from the transfer function provided by NWC. In this case, the temperature above ambient, in Kelvins, is given by

$$\frac{T_3}{\text{THRUST}} = \frac{4.48}{(1.233s+1)(50.76s+1)} \qquad (14)$$

where, as before, the thrust has the dimension of Newtons (see Fig. 6). A state-space equivalent of this expression, which is easily obtained by means of the MATRIXx function SFORM, is

$$\dot{\underline{x}} = \underline{A}\underline{x} + \underline{B}u$$

$$y = \underline{C}\underline{x} + \underline{D}u$$

where

$$\underline{A} = \begin{bmatrix} -0.8307 & -.0.0160 \\ 1 & 0 \end{bmatrix}, \quad \underline{B} = \begin{bmatrix} 1 \\ 0 \end{bmatrix}, \quad \underline{C} = [0 \quad 0.0716]$$

and $\underline{D}$ = 0. (In this representation, y is the shaft temperature T_3 and u is the thrust.) In the combined matrix format previously discussed in connection with Eq. (12), these matrices yield

$$\underline{S} = \begin{bmatrix} -0.8307 & -0.0160 & 1 \\ 1 & 0 & 0 \\ 0 & 0.0716 & 0 \end{bmatrix} \qquad (15)$$

The agreement illustrated in Fig. 9, which is clearly excellent, can be evaluated in several ways. For instance, the temperature response resulting from the identified system may be cast in a form that is directly comparable with that provided by NWC. To accomplish this, the system model may be converted to the 2-state matrix form given above, and the three parameters of $\underline{S}$ subjected to system identification. This has been done by means of the MAXLIKE procedure with the following result:

$$\underline{S}' = \begin{bmatrix} -0.8218 & -0.0173 & 1 \\ 1 & 0 & 0 \\ 0 & 0.0716 & 0 \end{bmatrix}$$

with a value of RSS = 63.4. Comparison of this result with Eq. (15) demonstrates the agreement. Using the TFORM command of MATRIXx, the state-space representation may be converted back to transfer-function form, yielding

$$\frac{T_3'}{\text{THRUST}} = \frac{4.13}{(1.250s+1)(46.08s+1)}$$

Comparing with Eq. (14) the agreement is, again, remarkable. The reader should bear in mind that these arguments are made here only for the purpose of demonstrating the effectiveness of the PSI procedure in this case. The various transfer functions and parameters in these models have no relation to the physical situation -- in fact, since they represent LTI systems, they are wholly inadequate for any purpose other than expressing the experimental measurements simulation

results in functional forms.

Several sets of initial values have been used in identifying the parameter values in the physical model, and the results have been found to be independent of this factor. In addition, a number of tests have been performed to determine the effect of varying other parameters in the system model and no significant improvement has been obtained on the results illustrated in Fig. 9. The selection of the appropriate parameters to vary in the PSI process requires some appreciation for the physical process modeled. Thus it has been observed, for instance, that the selection of too many parameters will lead to unrealistic values, such as negative thermal conductances, unless constraints are added to the MAXLIKE procedure. These and other aspects of the method are under continued study.

IX. CONCLUSIONS AND RECOMMENDATIONS

The emphasis in the work reported here has been to investigate the feasibility of using system identification methods to develop tools for use in the design of jet vane TVC devices. Before proceeding to conclusions in this regard, however, it may be useful to comment on the results obtained in the case that has been analyzed.

Results of the Analysis

The excellent agreement between measured and predicted shaft temperature responses shown in Fig. 9 gives some credibility to the model parameters used in the simulation.

These may in turn be related to vane physical properties to lend some insights regarding those quantities that were initially subject to relatively large uncertainties. For the heat sink effect of the shaft mount, for instance, the parameter $b_{33} = - a_{33} - a_{32}$ may be obtained from the identified value of $a_{33} = -0.46$ and the assumed (and relatively certain) value of $a_{32} = 0.38$. The result is $b_{33} = 0.08\ s^{-1}$ and this may in turn be related to the vane physical properties since $b_{33} = 1/C_3R_{3G}$. This new value is down from the original value of $0.10\ s^{-1}$ (Fig. 3), and, since RC = mcL/kA, the result may be used to adjust the rationale used in estimating the effective mass and geometry of the thermal sink representing the mount (assuming that the heat capacity and thermal conductivity are firm values).

The other parameter identified in the PSI analysis is the vane thermal input coefficient, $b_{33} = 0.2027\ s^{-1}$. If this value is used to recalculate the convective heat transfer coefficient, a value of $h = 638\ W/m^2K$ is obtained which is about 72% less than that estimated in Ch. IV for turbulent boundary layer convection. The conclusion, as has been mentioned, is that the complex processes of ablation and radiation account for a considerable amount of cooling of the vane. It is important to keep in mind that the single values quoted here are useful only inasmuch as they give good results for predicting shaft temperature response using the model that has been constructed. In this case, the model includes a ramp-up, plateau, ramp-down behavior for b_{33}

so that the above result, which applies to the plateau value of the "effective" heat transfer coefficient, accounts in a crude way for the fact that vane heat transfer effects vary widely throughout the firing. The assumption of a constant plateau value for h is, of course, subject to question and refinement if sufficient information is available.

Referring to the vane surface temperature responses shown in Fig. 9, it is seen that a maximum of about 1240K (950K above ambient) is reached at about 3.5 seconds (3 seconds after motor ignition). This value is well below the melting point of the vane material, and the tensile modulus is still about 22,000 ksi at this temperature (though it is well below the ambient value of about 45,000 ksi). It might be predicted from these results that the 1/4-scale vane that has been modeled would remain more-or-less intact during a firing of the type that has been simulated. A noteworthy feature of these developments is that it would be a relatively simple matter to simulate the thermal response of a full-scale vane. Each of the parameters in the present model is amenable to direct scaling procedures such as those that have been given in Ch. IV.

The PSI Method

The results thusfar obtained in this study justify some confidence that the thermal behavior of the jet vane can be modeled using a relatively simple and straight-forward model structure. But although the structure of the model is well defined, some of the values of the system parameters neces-

sary to make the model "work" are subject to considerable uncertainty. In this study the power of the system identification method has been brought to bear in removing some of this uncertainty. In addition, it is worth mentioning that the relatively new capabilities now available with software products like MATRIXx have greatly facilitated these advances.

Future research in these areas is warranted from both the modeling and system identification points of view. Using the model that has been developed here, or perhaps an even simpler model (without the tip node), it is important to determine if the good results obtained in the present instance can be expected in other cases. With this in mind, the results of other firing tests should be predicted with the model and further system identification conducted if it proves to be necessary. The basic issue would be to determine the robustness (or lack thereof) of the present model.

From the modeling point of view, a number of interesting questions remain of a more theoretical nature. The relationship between the complexity of the model and the adequacy of experimental comparison data is of some importance. In addition, more realism could be introduced into the present model in an effort to determine the sensitivity of the results to such matters. For instance, it might be possible to introduce a multiple thermal input model that accounts for radiation and ablation as well as thermal convection. Other elements of realism could be introduced by

allowing for the temperature dependency of several of the parameters now taken as constant. These include the thermal conductivity of the vane material and the reference temperature used in calculating the thermal properties of the motor exhaust gases.

Another aspect of the method that may lead to important insights is that the initial and final thermal responses seem to be somewhat uncoupled under the present circumstances. For example, the LTI response illustrated in Fig. 7 is quite adequate during the initial phase. The implication is that the initial and final transients might be used to identify particular parameter values under the assumption that they are time-invariant. If this were true, the handling of nonlinear behaviors, should this become necessary, would be greatly facilitated.

REFERENCES

1. National Aeronautics and Space Administration, "Solid Rocket Thrust Vector Control," NASA SP-8114, Lewis Research Center, Cleveland, OH, Dec., 1974.

2. Kampa, D., A. Weiss, and R. H. Schmucker, "Material Problems in Jet Vane Thrust Vector Control Systems," AGARD-CP-259.

3. Wirtz, D. F., "Preliminary Design and Performance Estimate of a Jet Vane Attachment in a Rocket Nozzle," internal memorandum 45701/DPW:cad, Reg. 45701-242-73, Naval Weapons Center, CA, 4 June, 1973.

4. Leitner, A., "Thrust Vector Control Heat Transfer Modeling," NPS69-86-005, Naval Postgraduate School, Monterey, CA, 1986.

5. Yukselen, A., "Heat Transfer Modeling of Thrust Vector Control Systems," MS Thesis, Naval Postgraduate School, Monterey, CA, 1986.

6. Spence, T. M., "Applications of Infrared Thermography in Convective Heat Transfer," MS Thesis, Naval Postgraduate School, Monterey, CA, March, 1986.

7. Nunn, R. H. and M. D. Kelleher, "Jet Vane Heat Transfer Modeling," NPS69-86-010, Naval Postgraduate School, Monterey, CA, Oct., 1986.

8. Dulke, M. F., "Heat Transfer Modeling of Jet Vane Thrust Vector Control (TVC) Systems," MS Thesis, Naval Postgraduate School, Monterey, CA, Dec., 1987.

9. Nunn, R. H., "Modeling of Jet Vane Heat-Transfer Characteristics and Simulation of Thermal Response," TTCP Panel W4, KTA9, Naval Postgraduate School, Monterey, CA, Sep., 1987.

10. Ziebland, H. and R. C. Parkinson, "Heat Transfer in Rocket Engines," AGARD-AG-148-71, AGARD, Sep., 1971.

11. Holman, J. P., Heat Transfer, 4th ed., McGraw-Hill, New York, 1976.

12. Turbulent Flows and Heat Transfer, ed. C. C. Lin, v.5, High Speed Aeronautics and Jet Propulsion, Princeton Univ. Press, 1959.

13. Private communication, Mr. John Gratcher, Code 3275, Naval Weapons Center, China Lake, CA.

14. Integrated Systems Inc., "MATRIXx/PC User's Guide,"

Palo Alto, CA, 1985.

15. ----, "SYSTEM_BUILD/PC User's Guide," 1986.

16. Borrie, J. A., Modern Control Systems: A Manual of Design Methods, Prentice/Hall International, Englewood Cliffs, N.J., 1986.

17. Integrated Systems Inc., "SYSTEM ID/PC User's Guide," Palo Alto, CA, 1986.

APPENDIX

Diagrams of System Build Super-Blocks

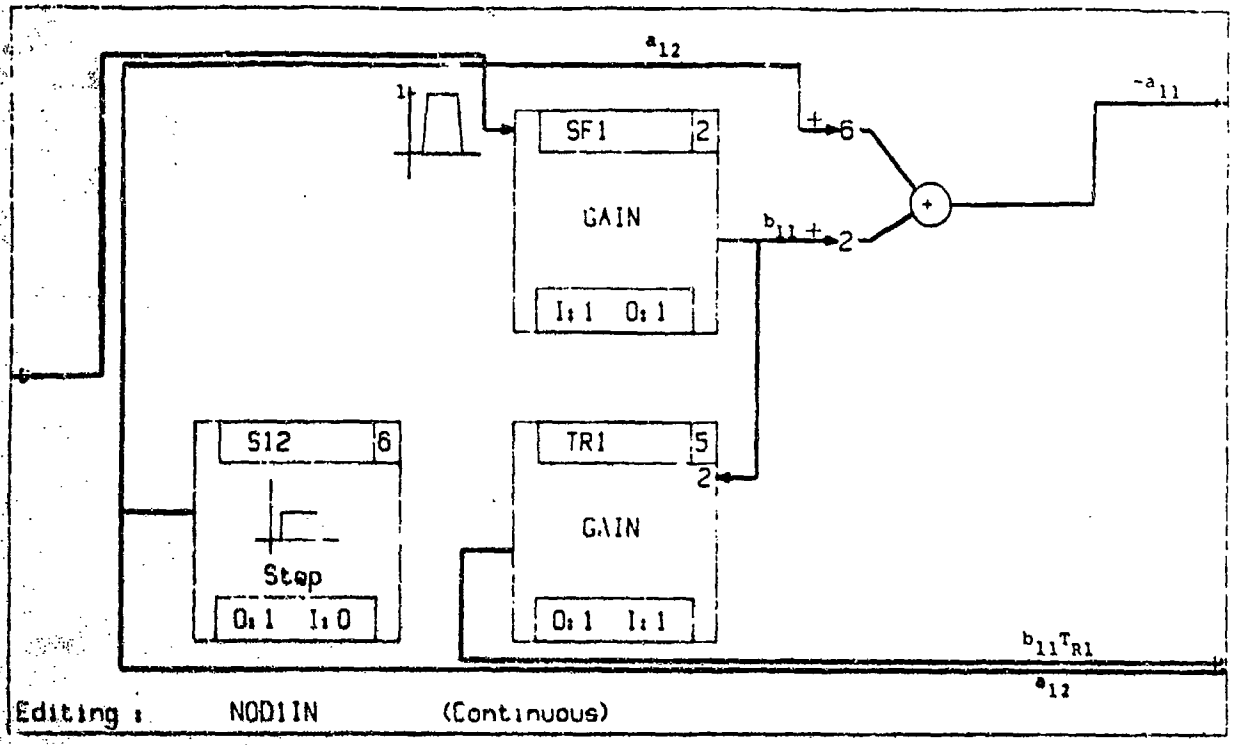
a_{12}
1
SF1
2
GAIN
I: 1 O: 1
b_{11}
+6
+2
$-a_{11}$
S12
6
Step
O: 1 I: 0
TR1
5
2
GAIN
O: 1 I: 1
$b_{11}T_{R1}$
a_{12}
Editing : NOD1IN (Continuous)

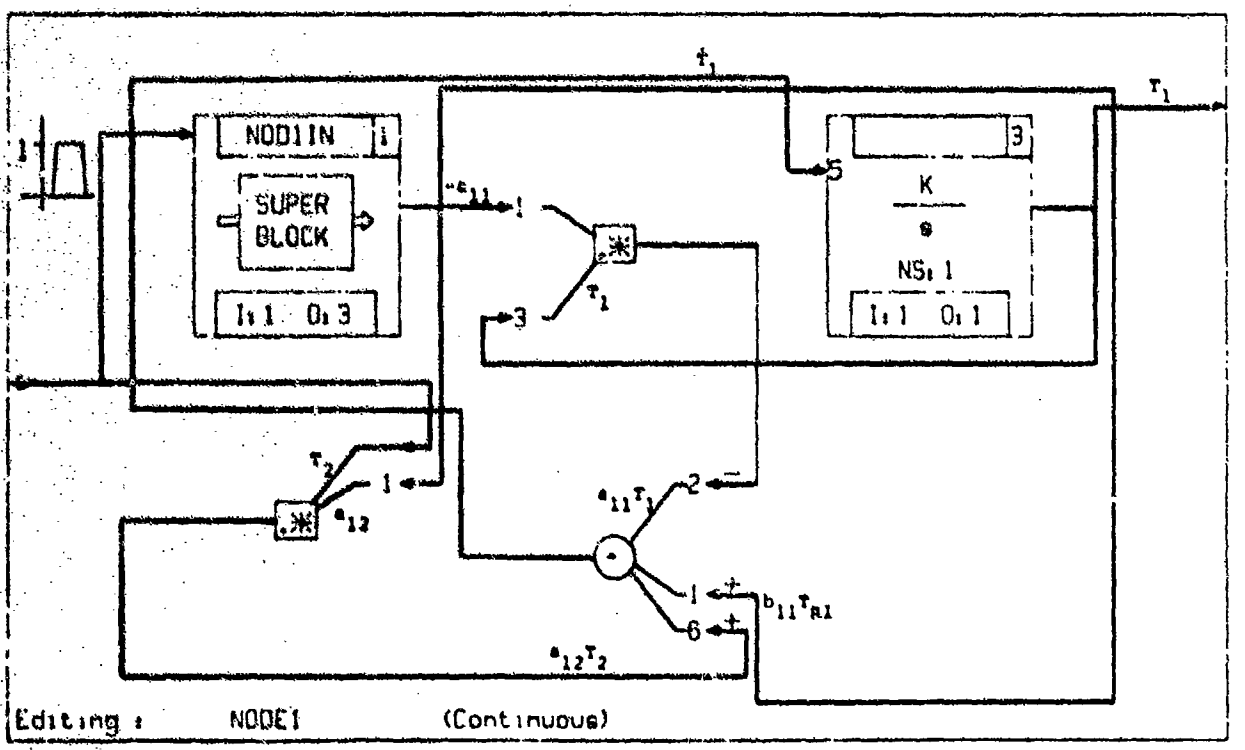
t_1
T_1
1
NOD1IN
1
SUPER BLOCK
I: 1 O: 3
$-a_{11}$
1
3
T_1
5
3
K
s
NS: 1
I: 1 O: 1
T_2
1
a_{12}
$a_{11}T_1$
2
1
6
$b_{11}T_{R1}$
$a_{12}T_2$
Editing : NODE1 (Continuous)

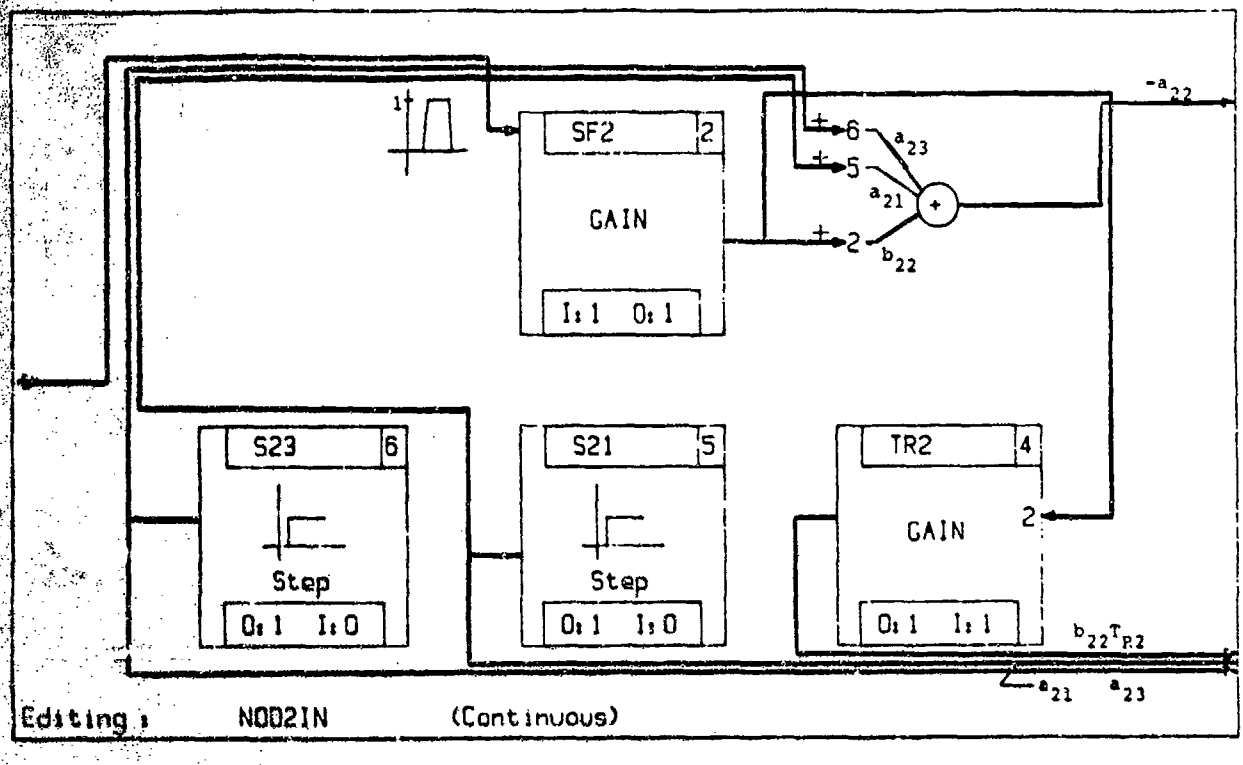
SF2
2
GAIN
I: 1 O: 1
S23
6
Step
O: 1 I: 0
S21
5
Step
O: 1 I: 0
TR2
4
GAIN
2
O: 1 I: 1
$-a_{22}$
a_{23}
a_{21}
b_{22}
$b_{22}T_{R2}$
a_{21} a_{23}
Editing : NOD2IN (Continuous)

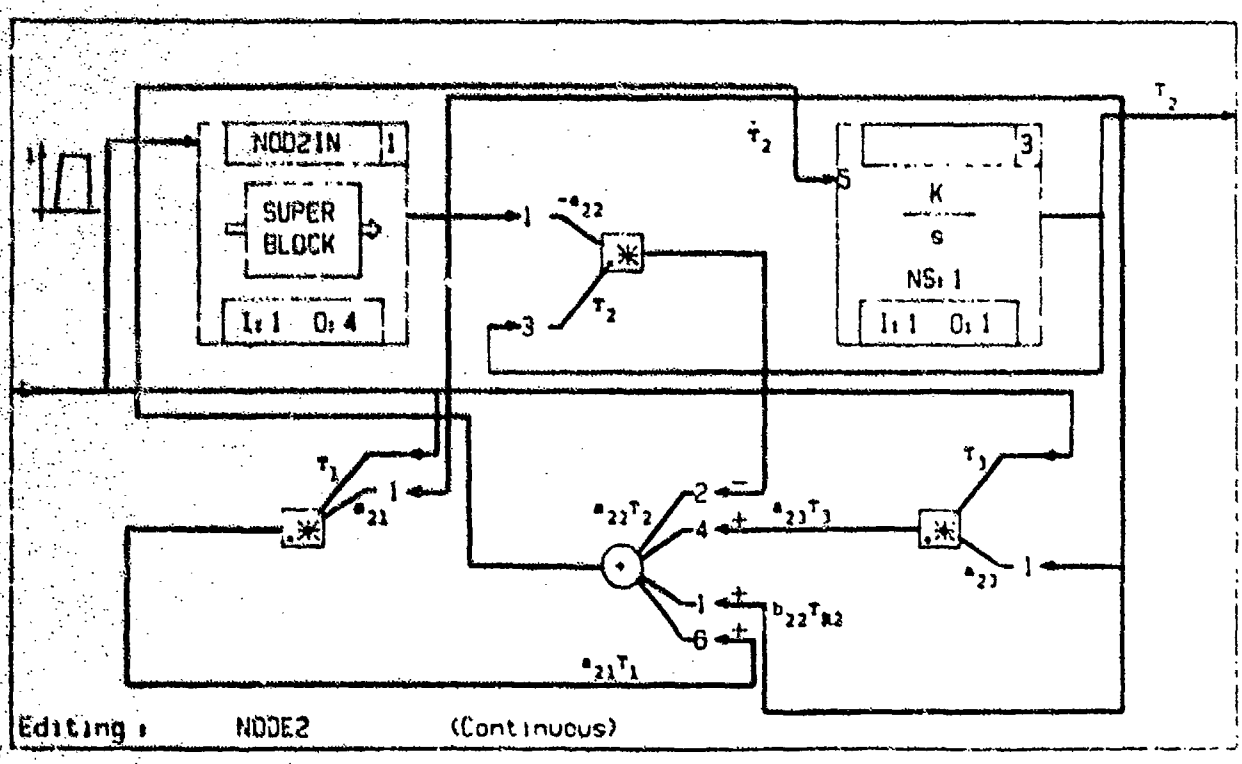
NOD2IN
1
SUPER BLOCK
I: 1 O: 4
$-a_{22}$
T_2
$\dot{T}_2$
3
K
s
NS: 1
I: 1 O: 1
T_2
T_1
a_{21}
$a_{22}T_2$
$a_{23}T_3$
T_3
a_{23}
$b_{22}T_{R2}$
$a_{21}T_1$
Editing : NODE2 (Continuous)

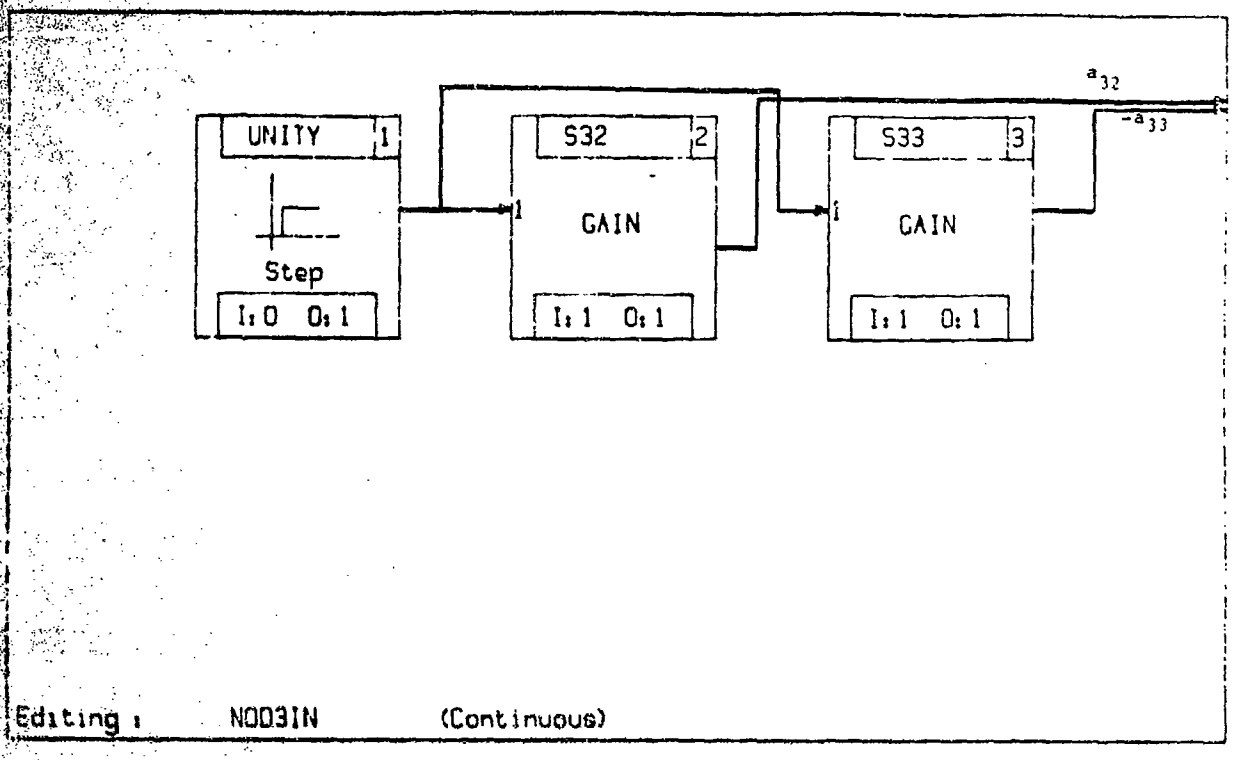
UNITY
1
Step
I: 0 O: 1
S32
2
GAIN
I: 1 O: 1
S33
3
GAIN
I: 1 O: 1
a_{32}
$-a_{33}$
Editing : NOD3IN (Continuous)

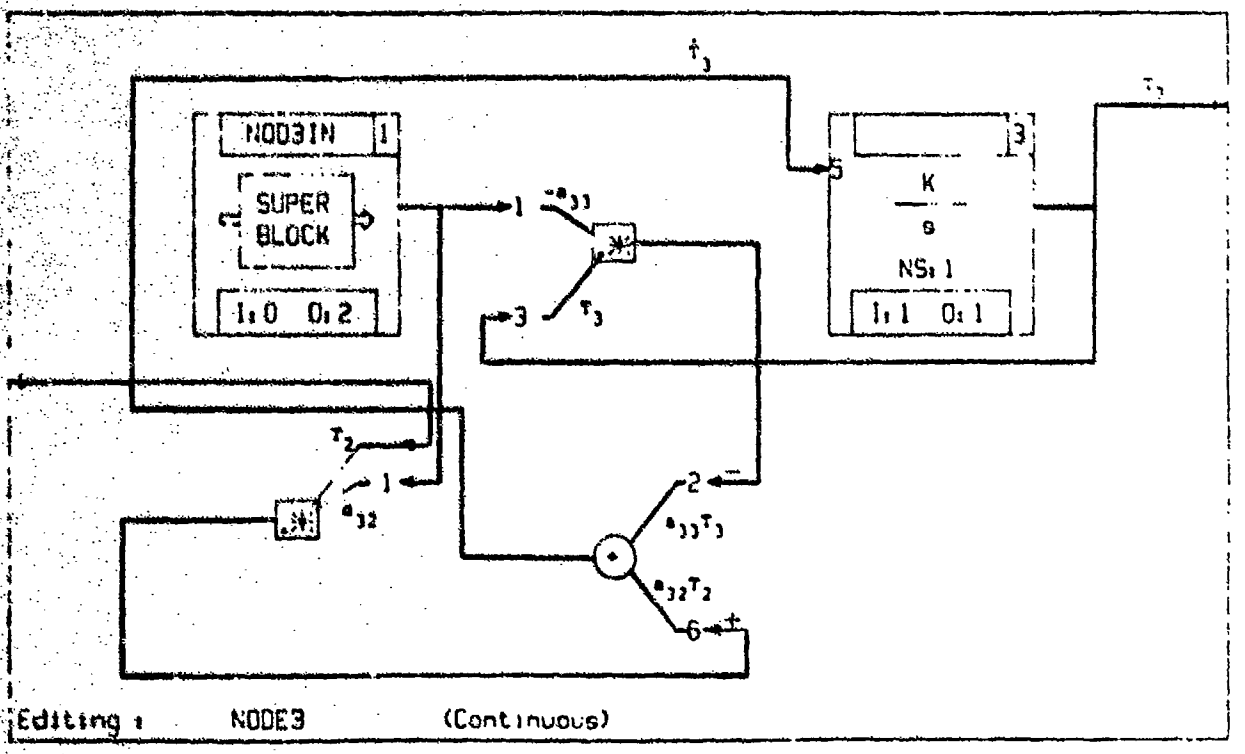
NOD3IN
1
SUPER BLOCK
I: 0 O: 2
$\dot{r}_3$
r_3
K
s
NS: 1
I: 1 O: 1
$-a_{33}$
r_3
r_2
a_{32}
$a_{33}r_3$
$a_{32}r_2$
Editing : NODE3 (Continuous)

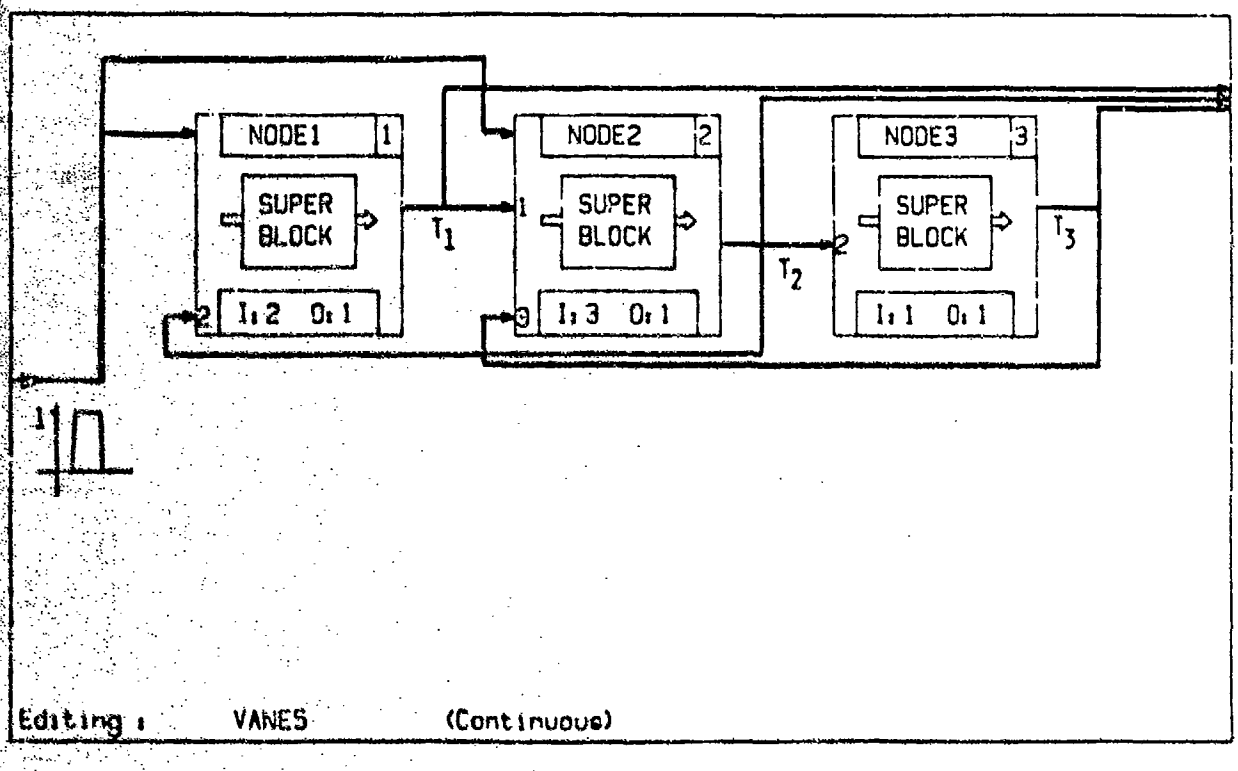

Editing : VANES (Continuous)

INITIAL DISTRIBUTION LIST

		No. Copies
1.	Library, Code 0142 Naval Postgraduate School Monterey, CA 93943-5100	2
2.	Research Administration, Code 012 Naval Postgraduate School Monterey, CA 93943-5100	1
3.	Chairman, Code 69 Department of Mechanical Engineering Naval Postgraduate School Monterey, CA 93943-5100	2
4.	Professor Robert H. Nunn, Code 69Nn Department of Mechanical Engineering Naval Postgraduate School Monterey, CA 93943-5100	10
5.	Professor L-W. Chang, Code 69Ck Department of Mechanical Engineering Naval Postgraduate School Monterey, CA 93943-5100	1
6.	Professor M. D. Kelleher, Code 69Kk Department of Mechanical Engineering Naval Postgraduate School Monterey, CA 93943-5100	1
7.	Professor P. Pucci, Code 69Pc Department of Mechanical Engineering Naval Postgraduate School Monterey, CA 93943-5100	1
8.	Professor D. Salinas, Code 69Sa Department of Mechanical Engineering Naval Postgraduate School Monterey, CA 93943-5100	1
9.	Professor D. Smith, Code 69Sm Department of Mechanical Engineering Naval Postgraduate School Monterey, CA 93943-5100	1
10.	Professor A. Gerba, Jr., Code 62Gz Department of Electrical and Computer Engineering Naval Postgraduate School Monterey, CA 93943-5100	1

INITIAL DISTRIBUTION LIST (continued)

	No. Copies
11. Professor H. Titus, Code 62Ts Department of Electrical and Computer Engineering Naval Postgraduate School Monterey, CA 93943-5100	1
12. Mr. Arne Danielson, Code 32731 Naval Weapons Center China Lake, CA 93555	5
13. Mr. R. Dillinger, Code 3273 Naval Weapons Center China Lake, CA 93555	1
14. Defense Technical Information Center Cameron Station, Alexandria, VA 22304-6145	2